ANNUAL REVIEWS

Annual Review of Condensed Matter Physics

The Hubbard Model: A Computational Perspective

Mingpu Qin,[1] Thomas Schäfer,[2] Sabine Andergassen,[3] Philippe Corboz,[4] and Emanuel Gull[5]

[1]Key Laboratory of Artificial Structures and Quantum Control, School of Physics and Astronomy, Shanghai Jiao Tong University, Shanghai, China

[2]Max-Planck-Institut für Festkörperforschung, Stuttgart, Germany

[3]Institut für Theoretische Physik and Center for Quantum Science, Universität Tübingen, Germany

[4]Institute for Theoretical Physics and Delta Institute for Theoretical Physics, University of Amsterdam, Amsterdam, The Netherlands

[5]Department of Physics, University of Michigan, Ann Arbor, Michigan, USA;
email: egull@umich.edu

ANNUAL REVIEWS **CONNECT**

www.annualreviews.org

- Download figures
- Navigate cited references
- Keyword search
- Explore related articles
- Share via email or social media

Keywords

quantum many-body theory, model Hamiltonians, strongly correlated electron systems

Abstract

The Hubbard model is the simplest model of interacting fermions on a lattice and is of similar importance to correlated electron physics as the Ising model is to statistical mechanics or the fruit fly to biomedical science. Despite its simplicity, the model exhibits an incredible wealth of phases, phase transitions, and exotic correlation phenomena. Although analytical methods have provided a qualitative description of the model in certain limits, numerical tools have shown impressive progress in achieving quantitative accurate results over the past several years. This article gives an introduction to the model, motivates common questions, and illustrates the progress that has been achieved over recent years in revealing various aspects of the correlation physics of the model.

1. INTRODUCTION

The Hubbard model is one of the simplest models of interacting fermions on a lattice. The model describes a fermion system with hopping term t and interaction strength U with Hamiltonian

$$H = -t \sum_{\langle ij \rangle \sigma} \left(\hat{c}_{i\sigma}^{\dagger} \hat{c}_{j\sigma} + \text{h.c.} \right) + U \sum_i \hat{n}_{i\uparrow} \hat{n}_{i\downarrow}, \qquad 1.$$

where i and j denote sites on a lattice; $\sigma = \uparrow, \downarrow$ enumerates two spin species; $\hat{c}$ and $\hat{c}^{\dagger}$ annihilate and create particles; $\hat{n} = \hat{c}^{\dagger}\hat{c}$; and h.c. denotes the Hermitian conjugate. Sometimes next-nearest-neighbor hoppings t' are also included. Physical observables and phase diagrams are typically examined as a function of temperature, chemical potential (or, correspondingly, density), or (staggered) magnetic field. In this form, the model goes back to papers by Hubbard (1), Kanamori (2), and Gutzwiller (3). As already noted by these authors, the model is a sketch of nature in that it emphasizes electron correlation physics caused by local interactions in a single orbital, whereas phenomena due to nonlocal interactions, band structure, or effects between multiple orbitals are not directly contained.

Despite these radical simplifications, the model has proven itself as a powerful tool for investigating correlated electron physics. On one hand, its relevance to cuprate physics has provided an early motivation for studying the model's phase diagrams and ground states. On the other hand, its simplicity has made it an ideal target for early quantum simulators, where many-body phenomena can be investigated without the complication of many of the effects present in realistic condensed matter systems.

Theoretically, the presence of metallic, insulating, ferro- and antiferromagnetic, superconducting, and charge-ordered phases in a model with very few parameters has proven an appealing test bed for new analytical methods. However, it became apparent early on that the standard analytical tool kit of condensed matter theory was insufficient to describe this rich physics to the desired accuracy and that sophisticated numerical methods would have to be used instead (4). This led to the development of a wide range of numerical tools based on many different approximations and approaches (5, 6), including diagonalization, diagrammatics, tensor network, variational, series expansion, Monte Carlo (MC) and embedding methods.

Although different approaches often led to different answers in earlier years, the situation has significantly improved more recently. Thanks to algorithmic advances and an increase of computing power, several methods have started to reproduce consistent results, leading to a growing consensus on various aspects of the Hubbard model. A phase diagram is provided in **Figure 1**.

1.1. Purpose and Structure of This Article

In this article, we review the recent progress in solving the Hubbard model from a computational perspective. We highlight results in which consensus has been reached among several numerical approaches and identify open challenges and their prospects of being resolved in the future.

Countless papers have been published on the Hubbard model over the past 30 years. Inevitably, our list of references and our selection of topics can therefore not cover all of the important developments in this field. A good starting point for references to additional numerical works is given by earlier reviews (8–13). An analytical perspective is provided in Reference 14 (in this volume).

Our main focus is the single-band Hubbard model on the two-dimensional (2D) square lattice with interactions ranging from weak to intermediate to strong coupling. We also make connections to the *t-J* model, which is an effective model of the Hubbard model in the large U/t limit, and the Hubbard model in three dimensions. In the remainder of this introduction, we define what we mean by "solving" the model and discuss its connection to experiments. We discuss the model
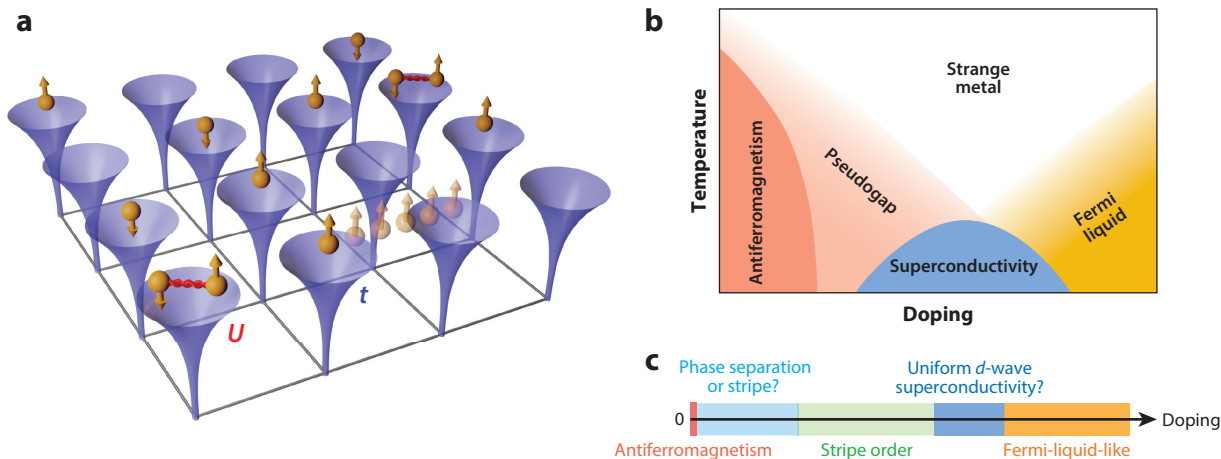
Figure 1

(*a*) Graphical representation of the Hubbard model. Two of many proposed phase diagrams of the model at intermediate interaction strength, at finite (*b*) and zero (*c*) temperature. Note (see Section 2) that panels *b* and *c* are mutually inconsistent: in panel *b*, charge-ordered phases are missing, and the precise locations of phases and boundaries are hotly debated; in panel *c*, the ground state in the large doped region is Fermi-liquid-like with an instability toward pairing through the Kohn–Luttinger effect (7).

in various parameter regimes, including broadly the weak coupling regime, which for the purpose of this article denotes interaction strengths $U/t \lesssim 4$ (rather than the mathematical limit in which weak coupling perturbation theory is exact); the intermediate coupling regime from $2 \lesssim U/t \lesssim 6$; and the strong coupling regime for $U/t \gtrsim 6$ (which includes regions outside the applicability of an infinite-U expansion).

We then review computational progress at half-filling (Section 3), before we consider the doped case at weak (Section 4) and intermediate to strong coupling (Section 5). Finally, we review the progress toward the simulation of experimental probes (Section 6). We only briefly discuss other lattice geometries, attractive interactions, multiorbital systems, nonlocal interactions, and extensions for nonequilibrium and driven systems (Section 7). We conclude by giving perspectives and stating open questions (Section 8). To limit the scope of this article, we also do not discuss the bosonic version of this model, which has been studied extensively with cold atomic gas systems.

1.2. "Solving" the Hubbard Model

Despite its simple Hamiltonian, exact solutions of the Hubbard model only exist in special circumstances. Therefore, as a practical definition, we define solving the Hubbard model as the task of obtaining results for a physically interesting observable to an accuracy that is comparable with or better than what is obtained in comparison calculations or experiments. Corresponding to the richness of the physics of the model, solving the model can therefore have a very different meaning depending on the observable and parameter regime considered, and over time the questions of interest as well as the precision with which they have been answered have changed.

For instance, the question of whether there is $d_{x^2-y^2}$ superconductivity in the Hubbard model at $U/t \sim 8$ and 1/8 doping, which has been a major controversy for decades, has only been conclusively answered in recent years, when several methods confirmed that the ground state exhibits stripes but no superconductivity. Although we consider this particular aspect as solved, there remains room for improvement on the quantitative level, such as higher accuracy on the magnitude of the stripe order.

It is frequently claimed, especially by works aiming to emulate the model in a quantum simulator or analog experiment, that the model is exponentially hard due to the negative fermion sign problem or the exponential scaling of the Hilbert space, and therefore not tractable in numerical studies. These statements are simplifications of the real challenge, which is that in order to obtain properties of the model, all methods, simulators, and emulators obtain a sequence of approximate solutions followed by an extrapolation to the exact limit. These may be finite-size extrapolations, extrapolations in the number of variational states kept or in diagram order, excitation level, final time for time-evolution, coherence time, and/or optical trap parameters. Many of these parameters are strongly linked to the physics occurring in a given parameter regime. Correspondingly, the quality and accuracy of all methods for the solution of the model strongly depend on the parameter regime studied.

Giving general guidance on the accuracy of the numerical and theoretical methods is difficult, as even small changes of parameters may turn an easy problem into a hard one, and vice versa. More importantly, advances in methodology steadily push the boundaries of the regions of phase space and observables that can be considered understood, and we expect similar progress to continue. Broad statements such as density matrix renormalization group (DMRG) only works for one-dimensional ground states or Monte Carlo cannot be used away from particle–hole symmetry due to the sign problem are mostly outdated.

In light of this it has been fruitful to establish multimethod consensus solutions (5, 6), defined as solutions obtained with two or more methods with different underlying approximations, where results for the same quantity at the same set of parameters agree within method uncertainties. **Figure 2** shows results from such benchmark projects. For a more detailed discussion of the respective errors of many of the numerical methods discussed here, we refer the reader to Reference 5 and references therein.

Collaborative benchmark projects have shown the value of obtaining results for the same parameters with multiple techniques. Even though several of the methods available are controlled or numerically exact in the sense that they converge to the exact result upon extrapolation in one or several parameters, this extrapolation is often difficult to perform in practice or the methods are applied outside of the regime in which the control parameters are small. Additionally, even though several techniques are uncontrolled in the sense that there are residual errors that cannot be extrapolated away, those errors may not be large when compared with the corresponding extrapolation or statistical uncertainties in controlled methods or the respective technique may be much better suited to a particular problem.

1.3. Connection of the Model to Experiments

Apart from its fundamental role as a paradigmatic model of correlated electron physics, connections of the Hubbard model to experiment have attracted additional interest. Particularly important are the connections of the model to cuprate physics and d-wave superconductivity, and the realization of the model by quantum emulators and quantum computers.

1.3.1. Cuprate physics.
Much of the interest in the Hubbard model in the intermediate to strong coupling regime stems from its relevance to the cuprate high-temperature superconductors discovered in the 1980s. Similar to experiments on these materials, Hubbard model simulations on the 2D square lattice find regions of parameter space with $d_{x^2-y^2}$ superconductivity, strong antiferromagnetic (AF) correlations, stripes, pseudogaps, Fermi liquid, and bad metallic behavior. Phase diagram lines and observables mirror many features of the experiment as a function of doping and temperature. However, it is difficult to make a precise correspondence between cuprate compounds and the single-orbital Hubbard model.
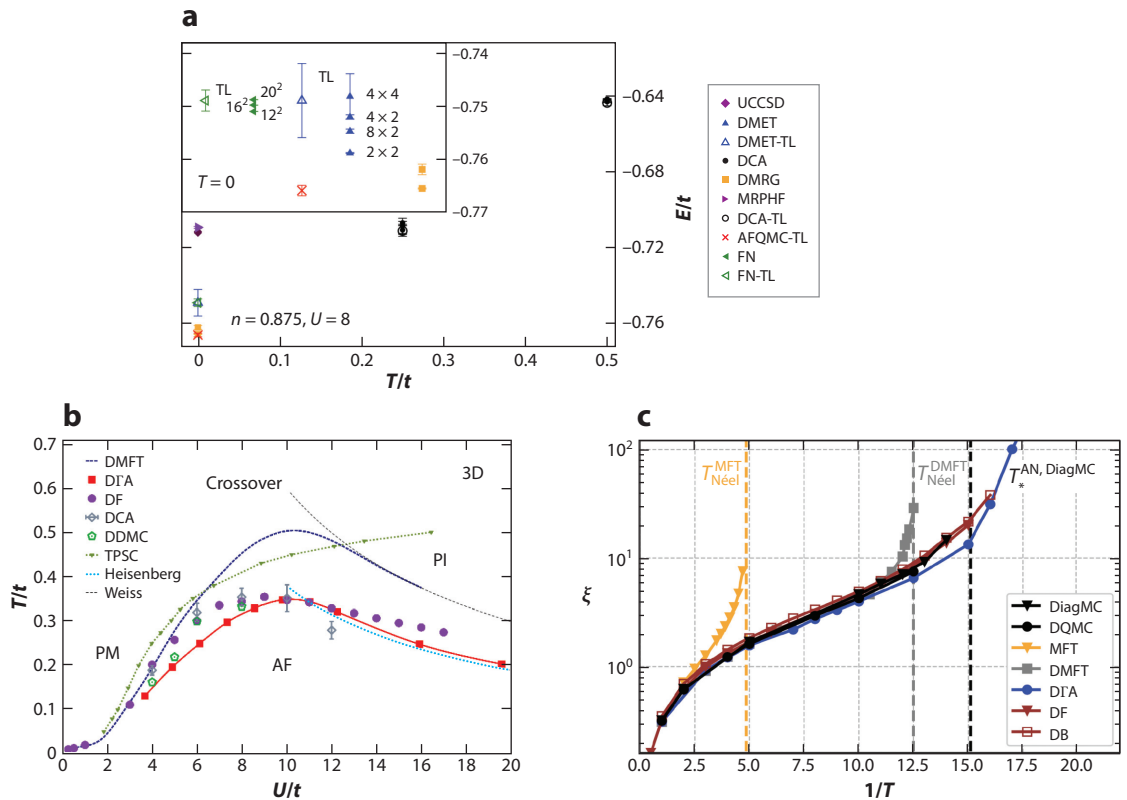
Figure 2

Consensus plots from benchmark studies of the Hubbard model. (*a*) Energy of the doped 2D square lattice model at $U/t = 8$ as a function of temperature. (*a, inset*) Results for the ground state energy. (*b*) Néel temperature of the half-filled model on a cubic lattice (with data from 15–20). (*c*) Weak coupling results for the temperature dependence of the magnetic correlation length ξ in the half-filled model on a 2D square lattice ($U/t = 2$). Panel *a* adapted from Reference 5. Panel *b* adapted with permission from Reference 21; copyright 2018 American Physical Society. Panel *c* adapted from Reference 6. Abbreviations: AF, antiferromagnetic insulator; AFQMC, auxiliary-field quantum Monte Carlo; AN, antinode; DΓA, dynamical vertex approximation; DB, dual bosons; DCA, dynamical cluster approximation; DDMC, determinantal diagrammatic Monte Carlo; DF, dual fermions; DiagMC, diagrammatic Monte Carlo; DMET, density matrix embedding theory; DMFT, dynamical mean-field theory; DMRG, density matrix renormalization group; DQMC, determinantal quantum Monte Carlo; FN, fixed node Monte Carlo; MFT, mean-field theory; MRPHF, multi-reference projected Hartree Fock; PI, paramagnetic insulator; PM, paramagnetic metal; TL, thermodynamic limit; TPSC, two-particle self-consistent approximation; UCCSD, unitary coupled cluster theory with single and double excitations.

Electronic structure simulations (22–26) and photoemission experiment (27) find bands with oxygen p and copper d character near the Fermi surface, necessitating a description with at least three orbitals (28). As Zhang & Rice argued (29), a superposition of oxygen and copper bands then yields an effective single-orbital model. The parameters t and t' can then be inferred by fitting the tight binding dispersion of a 2D square lattice with next-nearest-neighbor hopping to the ab initio band structure, leading to t'/t ranging from -0.1 to -0.4 for most hole-doped cuprates (23, 25, 26, 30). Parameters can also be fitted to experiment. Fits to the photoemission signal (27) at the Fermi energy E_F result in t' values of the same order and interactions of $U/t \sim 8$ (31). Similarly, the interaction parameter can be extracted by fitting the spin-wave dispersion of the model to results from neutron experiments (32).

These fits are neither systematic nor controlled. Nevertheless, they all yield interaction parameters comparable with the bandwidth, $U/t \sim 8$, and a small negative t'/t. A more accurate description of cuprate materials likely would include additional degrees of freedom such as multiple orbitals per site, nonlocal interactions, and additional nonlocal hopping terms.

Recent experiments on superconducting nickelate compounds have rekindled the interest in the high-temperature superconductivity aspect of the model (33). We also note that certain superconducting organic charge transfer salts may be described by a Hubbard model (34).

1.3.2. Quantum emulators and quantum computers. Due to the simplicity of the Hamiltonian, the richness of the physics, and the failure of analytical methods to provide adequate solutions, the fermionic Hubbard model is often chosen as a first target for analog quantum emulators (35). Hubbard quantum emulators aim to mimic the properties of the Hamiltonian by performing experimental measurements on a system that emulates the Hamiltonian. A wide range of emulators have been proposed, including (for the fermion model) ultracold atoms (36) and quantum dots (37–39). Although these systems do not reach the predictive power of numerical simulations in equilibrium (5, 6), interesting results have been obtained for time-dependent phenomena (40, 41).

An alternative route to quantum emulation is taken by early quantum computers (42). Here, one may hope that the simple interaction and hopping structure of the model may reduce complexity enough that quantum computers can provide solutions. Although current calculations lag far behind the capabilities of classical computers (43), results for Hubbard models in interesting parameter regimes will likely become available long before quantum computing solutions of materials or chemistry problems are possible (44).

2. PHASE DIAGRAM AND PHASE BOUNDARIES

Not much is known about the precise phase diagram of the Hubbard model in two dimensions. Although the ground-state phase diagram of the model at weak coupling is fairly well understood (45, 46), the phase diagram in the intermediate to strong interaction limit is hotly debated. Determining precise phase boundaries is hindered by the facts that the divergent correlation length at continuous phase transitions complicates finite-size scaling; that several competing phases have large and distinct unit cells; that energetic differences of competing phases are often minute; and that areas of phase space with very different physical properties are separated by broad crossovers, rather than sharp or first-order transitions. In addition, approximate methods tend to break symmetries and overemphasize ordered phases. For instance, though the Mermin–Wagner theorem (47) forbids magnetic order at nonzero temperature, most finite-size methods predict spurious magnetic phases that only disappear slowly in the limit of very large systems (48).

Correspondingly, though a broad consensus exists on the phases and their approximate locations, the precise shape of the transition lines is often not known. Visual representations such as the one in **Figure 1** therefore either correspond to the results within a given approximation or are inspired by comparisons to simple theories or experimental target systems.

The presence of so many orders and phenomena has led to the term intertwined orders (49), which is used in this context to express the fact that many different orders and phenomena either coexist in the same phase or are otherwise very close in energy or parameter space, making it difficult to pinpoint the exact location and properties of each phase.

In the following, we discuss some of these phases and their locations in parameter space. Numerous additional and exotic phases, including nematic phases, have been proposed for the Hubbard model. Reference 14 provides an overview and discusses some of these phases in more detail.

3. THE HUBBARD MODEL AT HALF-FILLING

3.1. The Two-Dimensional Model at Half-Filling

The fermion sign problem is absent in MC simulations of the half-filled Hubbard model on bipartite lattices (50). This makes efficient quantum Monte Carlo (QMC) simulations on large lattices possible, by either directly simulating finite-size systems or embedding cluster impurity problems with quantum embedding methods (10). Both results can then be extrapolated to the exact thermodynamic limit. Precise results are also available from other methods, see, e.g., References 5 and 6 for an overview of many physical quantities from a wide range of numerical methods.

3.1.1. Static quantities: energies, entropies, and spatial correlation functions.
The main static quantities of interest are ground-state and finite-temperature expectation values of energies and entropies, as well as spin and charge correlation functions. These quantities have been computed with a multitude of methods, and we summarize just a small selection of the results available.

Early finite-lattice QMC results for AF order parameters and energies for different U are presented in References 51 and 52, a thorough study of magnetic properties on large systems was performed in Reference 53, and a list of ground state energies from the diagonalization of 4×4 systems at various interaction strengths and for different electron numbers can be found in Reference 54. More recently, ground state energies, double occupancies, and AF order parameters for different interactions extrapolated to the thermodynamic limit were presented in Reference 55, calculated from a finite-size scaling analysis with twist-averaged boundary conditions. This work also tabulates finite-size data from 4×4 to 16×16 systems for different boundary conditions.

Short-range correlation functions at half-filling were calculated by QMC (56), and finite-temperature results can be found in Reference 53. In Reference 57, spin and charge correlations at finite temperature for $U/t \leq 4$ are calculated in a complementary diagrammatic Monte Carlo (DiagMC; 58) approach. Entropy and specific heat for the same approach (also for the doped case) can be found in Reference 59. In the weak coupling regime, the magnetic correlation length ξ grows exponentially when lowering the temperature (see **Figure 2c**; 6, 52, 60–63). Eventually, these long-range fluctuations are responsible for the destruction of magnetic ordering (Mermin–Wagner theorem; 47) and the development of a weak coupling pseudogap (see Sections 3.1.3 and 4.2) when approaching the (AF ordered) ground state from finite T.

3.1.2. Dynamical quantities: spectral functions.
The calculation of dynamical (i.e., frequency-dependent) results is considerably more challenging than the calculation of static observables. MC methods formulated in imaginary time or Matsubara frequency provide dynamical quantities, such as single- and two-particle spectral functions, via analytic continuation (64; see 50 for gap extraction at half-filling). This continuation is ill conditioned and introduces additional uncertainty into the spectra even at half-filling, where the sign problem is absent. In contrast, tensor network methods usually rely on a real-time evolution of the Hamiltonian, which avoids continuation but is limited by the growth of the entanglement with time, requiring increasingly large bond dimension. Alternatively, excitation spectra can also be obtained based on a tensor network excitation ansatz (65).

In the half-filled Hubbard model on the square lattice, QMC results for single-particle gaps at $U/t = 4$ were calculated in References 66 and 67. In Reference 68, single-particle gaps for different interactions were obtained in the thermodynamic limit by a careful finite-size analysis, establishing the presence of a gap for all interactions with an exponential decay in the small U limit and linear scaling for large U.

Complementary results are provided by tensor network methods. In Reference 69, the spectral function was obtained using time-dependent DMRG (70) as a solver in cluster perturbation theory for clusters up to 2×80, which agreed with earlier QMC results (71–74), but with a higher resolution. Time-dependent matrix product state (MPS; 75) calculations of spectral functions on four-leg and six-leg cylinders have so far only been obtained for the *t-J* model (76). In Reference 65, results for the excitation gaps for $U/t = 12$ were obtained based on an MPS excitation ansatz on four-leg and eight-leg infinite cylinders.

Resolving the full frequency and momentum dependence of the spectral function in the Brillouin zone is a difficult outstanding problem. Results from cluster dynamical mean-field theory (DMFT; 77) are available at selected momentum points or averaged over small areas in momentum space (see, e.g., 78), but extracting the detailed momentum dependence and Fermi surface shape yield results that strongly depend on the periodization schemes employed (79).

3.1.3. Nature of the gap.
The ground state of the 2D Hubbard model on a square lattice with $t' = 0$ is insulating; i.e., it has a charge gap for any interaction strength U (50, 52, 62, 68, 80). AF Néel order (51, 53) persists for all interaction strengths.

In the strong interaction limit, the gap is of the Mott type (81), and the low-energy physics is described by an effective spin-1/2 Heisenberg model with coupling constant $J = 4t^2/U$ (82). The origin of the gap in the weak interaction region was controversial, and Reference 83 argued that the gap in the weak interaction limit remains Mott. A complementary view is provided by the Slater mechanism (84), where the gap is formed by the establishment of long-range Néel order due to the perfect nesting of the Fermi surface.

A diagnostic is provided by the evolution of the potential and kinetic energies as a function of interaction and temperature. In a Mott system, the transition to the insulator is accompanied by a lowering of the kinetic energy, whereas the Slater mechanism lowers the potential energy (63, 85). Whereas early dynamical cluster approximation (DCA; 10) calculations (86) supported Mott, later studies (57, 62, 63, 85) found a decrease of the potential energy in the weak coupling region, supporting a Slater mechanism. Despite the differing origins of the gap in the weak and strong coupling region, no phase transition between the two regimes is observed, indicating a crossover near $U/t \approx 4$ (57, 68), which agrees with the properties of the underlying ground state. Like the Heisenberg model (87, 88), below the charge gap, the Hubbard model is well described by a 2D quantum nonlinear sigma model (89, 90), with strong renormalizations, e.g., of the spin-wave velocity.

The evolution of the gap size and AF correlation length with temperature is difficult to study in numerical simulations, even where the sign problem is absent, as the spin correlation length grows exponentially when temperature is decreased. Rich physics is found in this process: Upon cooling toward the insulating AF ground state, a sequence of crossovers among a high-temperature incoherent regime, an intermediate metallic regime with coherent quasiparticles, and a low-temperature insulating regime with an AF pseudogap (57, 62, 80) is observed in dynamical vertex approximation (DΓA; 21), QMC, and DiagMC. Due to the increased scattering rate at low T, the inverse quasiparticle lifetime (extracted from Matsubara data) shows a minimum as a function of temperature (63, 91). Results for further observables from different methods at weak coupling can be found in Reference 6.

3.2. The Half-Filled Model in Three Dimensions

For all interaction strengths, the half-filled model with $t' = 0$ in three dimensions exhibits a phase transition from a paramagnetic state at high T to an AF insulator at low T. The maximum transition

temperature of $T_N/t \sim 0.35$ occurs near $U/t \sim 8$, remains large in the interval of $7 < U/t < 10$, and decays rapidly for both weak and strong coupling (17–18, 21, 92; see **Figure 2b**). In addition to the AF phase transition, the system also exhibits a crossover identified by a change in either the compressibility or the density of states at the Fermi energy near $U/t \sim 6$–8 (16, 93) between metallic (at weak coupling) and insulating (at strong coupling) behavior in the high-temperature phase.

Lattice MC methods (94) and cluster quantum impurity solvers (95) do not suffer from a sign problem, and accurate results for the system are available for all interaction strengths (18, 20, 96). The accurate treatment of the continuous phase transition requires considerable care due to the divergent length scale of fluctuations at the phase transition, and the transition has therefore been used as a rigorous test for diagrammatic extensions of the DMFT (17, 19, 21) and for finite-size effects in cluster methods (18, 20, 97). Critical exponents have been studied with diagrammatic extensions of DMFT (17, 19, 98) and, within those approximations, are compatible with Heisenberg universality for all interaction strengths.

The three-dimensional system is of particular interest in the context of cold Fermi gases (99, 100), where cooling toward an ordered state in three dimensions proved less challenging than probing 2D superconducting and AF correlations, mainly due to the high critical temperature of the model. Entropy, rather than temperature, is conserved in closed traps, and the highest critical entropy of $S \sim 0.65$ lies near $U \sim 8t$ (97). Entropies of 0.77 were reached in Reference 101; AF correlations were observed in References 102 and 103, and lattice cold atom experiments have since steadily increased the accessible parameter space (104).

4. THE DOPED TWO-DIMENSIONAL HUBBARD MODEL AT WEAK COUPLING

4.1. Magnetic and Superconducting Properties

The ground state phase diagram reveals rich behavior as a function of the different parameters. In addition to AF Néel order, magnetic order with generally incommensurate wave vectors away from the Néel point (π, π) can be found away from half-filling in mean-field studies (105–108) and, including fluctuations, by expansions in the hole density (109–112). Incommensurate magnetic order is also indicated by diverging interactions and susceptibilities in functional renormalization group (fRG) flows (113–115), where approximate solutions indicate robust magnetic order up to fairly high doping provided that superconductivity is suppressed (116).

Although the magnetic instability in the Hubbard model is reproduced already by conventional mean-field theory, pairing is fluctuation-driven and, hence, more difficult to capture. Simple qualitative arguments suggesting d-wave pairing driven by magnetic fluctuations were corroborated by the fluctuation exchange approximation (117). Convincing evidence for superconductivity at weak and moderate-coupling strengths has been established by self-consistent or renormalized perturbation expansions (118–121) and DiagMC (45, 122) and from fRG calculations (113, 115, 123–126). With its unbiased treatment of all fluctuation channels on equal footing, the fRG confirmed earlier studies based on the summation of certain perturbative contributions (13), finding d-wave superconductivity with a sizable gap for a finite next-nearest-neighbor hopping amplitude (126) coexisting with Néel or incommensurate antiferromagnetism in a broad doping range (116, 127, 128). When the chemical potential approaches the van Hove singularity, different instabilities compete: Besides spin-density wave and pairing instabilities, ferromagnetism has been observed at moderate $|t'/t|$ (119, 121, 125, 129–131). At finite temperature, computing the Kosterlitz–Thouless (KT) transition temperature from the superfluid phase stiffness, a superconducting dome centered around optimal doping has been found (132). Recently, fRG flows starting from the DMFT

solution instead of the bare action (DMF^{2}RG; 133, 134) confirmed robust pairing with d-wave symmetry at strong coupling, driven by magnetic correlations at the edge of the AF regime.

4.2. Weak Coupling Pseudogap

The term pseudogap refers to a momentum-dependent suppression of the single-particle spectral function near the Fermi energy. In contrast to the pseudogap originating from strong coupling effects (see Section 5.2), at weak to intermediate coupling the pseudogap is induced by long-range AF correlations (6, 89, 135–137). The gap opens when the correlation length exceeds the thermal de Broglie wavelength $\xi \gg v_F/(\pi T)$, where v_F is the Fermi velocity (135). The phenomenon has been studied within the two-particle self-consistent approach approximation (135), the DΓA (62), the dual-fermion approach (138), the parquet approximation (139), the DiagMC (80), and the fRG (140).

The underlying mechanism can be understood already from the second-order contribution of the self-energy: Using the Ornstein–Zernike form for the spin susceptibility, it predicts a spectral gap for momenta close to the hot spots where the Fermi surface crosses the magnetic Brillouin zone boundary (135, 141). Upon lowering the temperature, the gap opens first near $(\pi, 0)$ (the so-called antinode), then spreads across the Fermi surface until also the region near $(\pi/2, \pi/2)$ (the so-called node) becomes insulating. Although a momentum-selective gap opening due to long-range AF spin fluctuations has been observed also at electron doping (11, 136, 142), most studies focus on models with a finite next-nearest-neighbor hopping t', which show a non-Fermi liquid behavior of the self-energy at hole doping. In the weak coupling regime, there is a natural connection between the Fermi surface topology and the coherence of low-energy quasiparticles: For a hole-like Fermi surface, the coherence of low-energy quasiparticles is suppressed at the hot spots. When the Fermi surface turns electron-like, increased quasiparticle coherence is restored all along the Fermi surface. The pseudogap only exists when the Fermi surface is hole-like. Hence, the Lifshitz transition from hole- to electron-like topology controls both the location of the self-energy singularities and the topological transition of the Fermi surface.

5. THE DOPED TWO-DIMENSIONAL HUBBARD MODEL AT INTERMEDIATE TO STRONG COUPLING
5.1. Competition of Low-Energy Ground States: Uniform Versus Stripe States

A striking feature of the doped 2D Hubbard model at strong coupling as well as of the t-J model is that they exhibit several competing ground states that lie very close in energy. This includes, on the one hand, a uniform d-wave superconducting state (see References 8–12 for a review of early results) sometimes coexisting with AF order at low doping, and on the other hand, various inhomogeneous states in which charge and/or spin densities are modulated, called stripes (see 49, 143–145 for reviews). Experimentally, stripe order was also observed in some cuprate materials (146) in the underdoped region. In early Hartree–Fock and analytical studies, stripes were found to be insulating with a filling of exactly one hole per unit length (147–151), whereas later it was found that stripes may also exhibit a different hole density (152–154) with coexisting d-wave superconductivity (155–160). A more complex variant of the stripe, called a pair-density wave (PDW) state (145), includes a π phase shift in the superconducting order between neighboring stripes, such that d-wave superconductivity vanishes on average. The PDW state was proposed in Reference 161 as a possible explanation for the suppressed superconductivity observed in lanthanum barium copper oxide (LBCO) around $\delta = 1/8$ doping (162), which is energetically very close to the stripe without phase shift (156, 159, 163).

Due to this strong competition, it has been an open question for many years whether the ground state is a uniform d-wave or a stripe state (with possible coexisting superconductivity). Initially, the former was supported particularly by many variational Monte Carlo (VMC) studies (164–170) and (cluster) DMFT studies (48, 113, 171, 172). A common opinion was that the stripes found with DMRG could be an artifact of the cylinder geometry and that they would not be stable in isotropic, periodic systems (which are difficult to study with DMRG). This viewpoint was supported by a VMC study (173), where it was shown that a lattice anisotropy indeed leads to (spin) stripe correlations, and also by Reference 174, where no stable stripe state was obtained in the t-J model, even when adding a (period 4) stripe bias and combining VMC with fixed-node MC and Lanczos steps. By contrast, stripe states were found with infinite projected entangled-pair states (iPEPS; 175) in the 2D thermodynamic limit (158) in the t-J model, which are energetically lower, but very close to the uniform state (159), in a (constrained-path) auxiliary-field quantum Monte Carlo [(CP-)AFQMC; 176] calculation (177), and also in an inhomogeneous DMFT approach for $U/t = 8$ (178).

More recently, based on a combined study with DMRG, CP-AFQMC, density matrix embedding theory (DMET; 179), and iPEPS, consensus has been reached that the ground state of the doped 2D Hubbard model for $U/t = 8$ ($t' = 0$) and $\delta = 1/8$ doping is a stripe state with a charge period of 8 without coexisting d-wave superconducting order (180; see **Figure 3c**). Although stripes with periods of 5–7 and coexisting d-wave superconductivity are energetically very close to the period 8 stripe, the uniform d-wave state is higher in energy by $\approx 0.01t$ (see **Figure 3d**). The estimates of the energy for the period 8 stripe obtained from the four methods are in remarkably close agreement, lying at about $-0.767 \pm 0.004t$. The period 8 stripe remains also stable in an extended interaction range ($U/t \sim 6$–12), where the energy difference with respect to other stripes becomes larger with decreasing U/t; i.e., the strongest competition is found for $U/t = 12$ (whether the stripe period shifts to lower periods at even larger U/t is still an open question). Subsequently, the stripe ground state has been confirmed by VMC (181, 182), in determinant QMC (183), in other DMRG studies (183–186), and by a variational AFQMC approach (187). The main reason why in previous VMC calculations (174) stripe states were found to be higher in energy than uniform states is that only a period 4 stripe was considered, which is substantially higher in energy than the period 5–8 stripes (180, 182). This resolves the previous discrepancy and also highlights the importance of using the correct unit cell in these calculations.

Moving away from $\delta = 1/8$ doping, several approaches predicted that the stripe period decreases with increasing doping (see, e.g., 181, 182, 187, 188), with a tendency to stabilize insulating, fully filled stripes of period λ at doping $\delta = 1/\lambda$ (for $U/t = 8$, $t' = 0$). For dopings in between these fully filled stripes, partially filled stripes with coexisting superconductivity have been found by VMC (182), whereas variational AFQMC predicted phase separation between insulating stripes (187). Based on a combined DMRG and CP-AFQMC study, it was concluded that superconductivity in the stripe ground state is absent over an extended doping ($\delta \sim 0.1 - 0.2$) and interaction ($U/t \sim 6$–8) range (189). At low doping, phase separation between the AF state at half-filling and a partially filled stripe was found to occur around $\delta \approx 0.08$ for $U/t = 8$ (182, 187) [$\delta \approx 0.07$ for $U/t = 10$ (188)], but a confirmation of this result with tensor network methods or CP-AFQMC is still lacking. [We note that the possibility of phase separation at low doping (190) was already intensely studied many years ago (see 8, 191 for reviews), but this concerned phase separation between the AF state and the uniform d-wave state.]

The fate of the uniform d-wave state, i.e., under what conditions it is favored over stripe states, is an important question but has not been investigated by all methods. The VMC study in Reference 182 predicted a stable uniform d-wave region in a doping range of $0.20 \lesssim \delta \lesssim 0.27$, for $U/t = 8$ ($t' = 0$), whereas a doping range $0.19 \lesssim \delta \lesssim 0.22$ was found with variational AFQMC (187).

VMC: variational Monte Carlo

iPEPS: infinite projected entangled-pair states

(CP-)AFQMC: (constrained-path) auxiliary-field quantum Monte Carlo

DMET: density matrix embedding theory
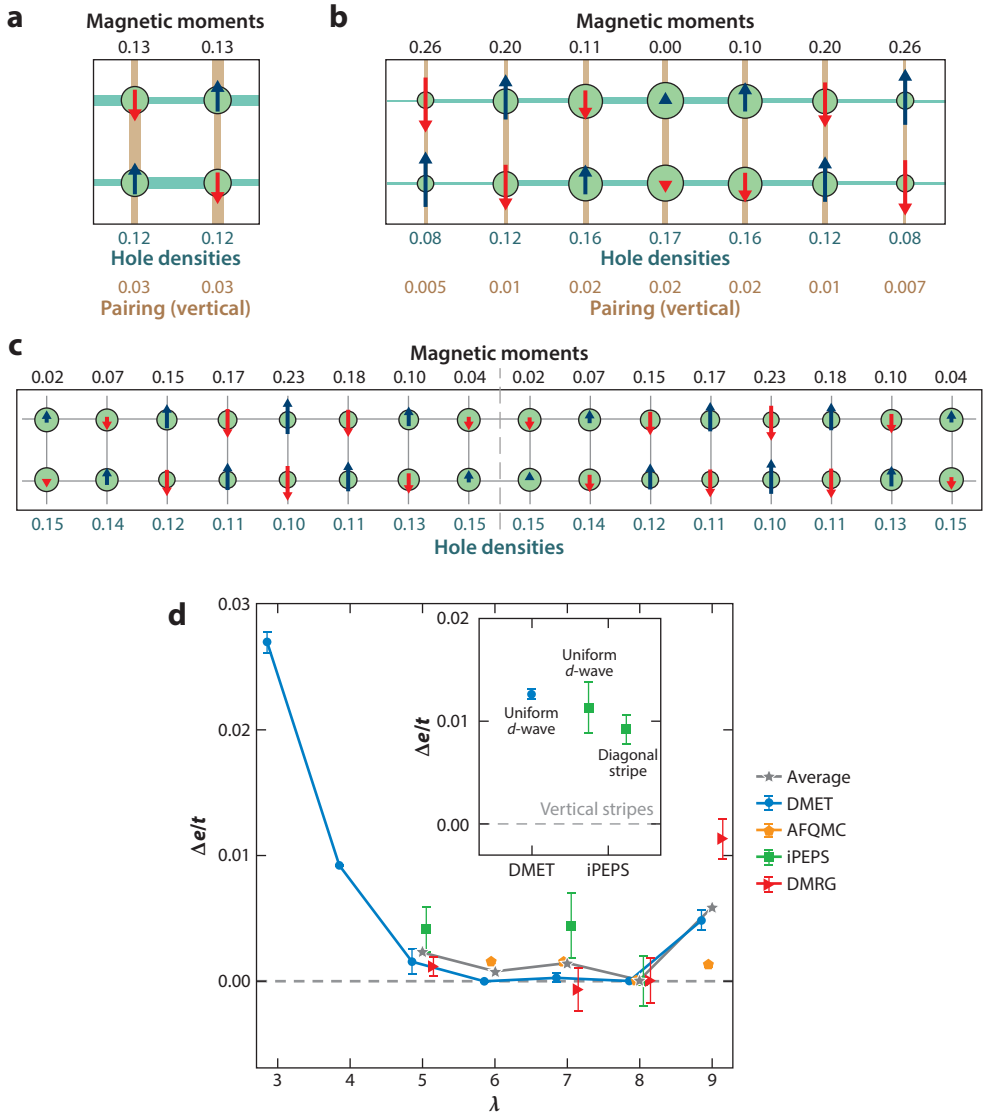
Figure 3

(*a–c*) Examples of competing states in the doped 2D Hubbard model for $U/t = 8$ and $\delta = 1/8$. The circle radius and the arrow length are proportional to the hole and spin densities, respectively, and the width of the colored bonds scales linearly with the local singlet pairing strength. (*a*) Uniform *d*-wave superconducting state with coexisting AF order (from iPEPS). (*b*) A stripe with charge and spin period 7 with coexisting *d*-wave superconductivity, and the typical π-phase shift in the AF order across the domain wall with maximal hole density (from iPEPS). (*c*) A period 8 stripe with exactly one hole per unit length per stripe, where superconductivity is entirely suppressed (from CP-AFQMC). Note that due to the π-phase shift in the AF order, the period of the spin order is doubled in stripes with an even charge period. (*d*) Energies of stripes with different charge periods λ and the uniform *d*-wave state (*inset*) relative to that of the $\lambda = 8$ stripe obtained with different methods. Figure adapted from Reference 180. Abbreviations: AF, antiferromagnetism; AFQMC, auxiliary-field quantum Monte Carlo; CP-AFQMC, constrained-path auxiliary-field quantum Monte Carlo; DMET, density matrix embedding theory; DMRG, density matrix renormalization group; iPEPS, infinite projected entangled-pair states.

Based on an approach combining VMC and a tree-tensor network for $U/t = 10$ ($t' = 0$) (188), it was concluded that the uniform d-wave state gets stabilized for $0.17 \lesssim \delta \lesssim 0.22$. A similar approach was used in Reference 192 to study an ab initio effective one-band model for Hg-based superconductors, where it was found that the long-range Coulomb interaction stabilizes the uniform d-wave state over an even larger doping region, $\delta \gtrsim 0.1$, with a competing period 4 stripe only remaining around $\delta \sim 0.1$. These results suggest that, though the various competing states can already be observed on the level of the simplest Hubbard model, more accurate models with further-neighbor interactions and hoppings are required to quantitatively reproduce the phase diagram of the cuprates. At the same time, to better resolve the tiny differences in energy for these competing states, more accurate methods need to be developed.

5.1.1. Competition at intermediate U/t.
Although the stripe ground state is now well established at strong coupling $U/t \geq 6$, the relevance of stripes in the intermediate-coupling regime is still not settled. At $U/t = 4$, using DMRG and CP-AFQMC, the tendency for stripe formation was found to be weaker (189) than at large coupling. A uniform d-wave ground state for $U/t \leq 4$ and large doping $\delta \geq 0.3$ was predicted from DiagMC (45, 122); however, smaller dopings were not accessible due to convergence problems of the diagrammatic series. More work is needed to accurately identify the crossover regime between uniform and stripe states.

5.1.2. Stripes at finite t'.
Stripe ground states have also been found upon including a negative next-nearest-neighbor hopping t' (corresponding to the hole-doped case), where the preferred stripe period shifts to smaller values with increasing strength of $|t'|/t$ (181, 183, 185, 186, 193). (A sufficiently large positive $t'/t \gtrsim 0.15$, in contrast, stabilizes the uniform d-wave state over the stripe state; 183, 193.) Interestingly, a period 4 stripe, which is the typical period found in experiments (146), is stabilized at 1/8 doping over a wide range of t', $0.16(4) < |t'|/t < 0.423(10)$ (193; a similar lower bound was found in 181), which includes the values that have been predicted as realistic parameters for different cuprate materials (22, 25, 26). Both iPEPS (193) and VMC (181) predict period 4 stripes without coexisting d-wave order at 1/8 doping. However, in contrast to VMC, iPEPS finds coexisting d-wave superconductivity in the period 5–7 stripes at 1/8 doping, and in the period 4 stripe at larger doping $0.14 \lesssim \delta < 0.25$ (corresponding to a hole density per stripe unit length, $0.57 \lesssim \rho_l < 1$; a similar range was also found for the period 5 stripe). Coexisting superconductivity in the period 4 stripe was found on a width-4 cylinder using DMRG (185, 186, 194) (also in the t-J model; 195, 196); however, it was pointed out in Reference 194 that the pairing on the width-4 cylinder does not correspond to the ordinary d-wave order one would expect in the 2D limit but to a plaquette d-wave pairing. (Another difference between the width-4 cylinder DMRG and the iPEPS/VMC results is that in the former the spin order is not long ranged but only short ranged.) Clearly, the issue of coexistence or absence of superconductivity in stripe states and its nature (with or without phase shift between neighboring stripes) remains an important topic for future research.

5.1.3. Competition in three-band models of the cuprates.
A competition between different low-energy states can also be found in three-band Hubbard models with parameters relevant for the cuprates. Uniform d-wave superconducting states have been predicted in VMC (197–202), DMET (203), cluster DMFT (204), and DCA studies (205), whereas stripe states have been found in DMRG (206) and determinant QMC (fluctuating stripes at finite temperature; 207) studies. In the CP-AFQMC study in Reference 208, stripes with spin and charge orders were found for large values of the charge-transfer energy ($\delta = 4.4$ eV), whereas for small values ($\delta = 2.5$ eV) the charge order becomes weaker and a subtle competition between different spin orders was found.

Stripes coexisting with superconductivity have been predicted in a VMC study (198); however, a confirmation of this result with more recent techniques is still lacking.

5.2. Pseudogap

In cuprate materials, the so-called pseudogap appears for dopings smaller than optimal doping and temperatures below $T^* \sim 300$ K as a suppression of the density of states near the antinode $(\pi, 0)$ in the Brillouin zone but not near the node $(\pi/2, \pi/2)$. Originally it was identified as a suppression of the nuclear magnetic resonance (NMR) Knight shift (209). However, signatures of the pseudogap are found in a wide variety of other probes (210), in particular angle-resolved photoemission spectroscopy (211, 212). Experimental correlation lengths are estimated to be on the order of a few lattice spacings (213). Therefore, the corresponding parameter regime in the Hubbard model is most often studied with cluster methods such as DCA and cellular dynamical mean-field theory (CDMFT; 10), as these methods capture short-range correlation well and provide access to spectral functions.

5.2.1. Results from cluster dynamical mean-field theory.
Pioneering results demonstrated that the inclusion of short-ranged correlations is sufficient to describe the suppression of the antinodal density of states in the single-particle spectral function upon lowering $T < T^*$ (214–216; **Figure 4a**). These DCA results were corroborated by 2×2 CDMFT calculations with various impurity solvers, and their temperature, interaction, doping, and band structure (t, t') dependence were explored (11, 218–222). For instance, Reference 219 showed that, in addition to the strong renormalization of the Fermi surface at small dopings, there is a fundamental asymmetry of systems with negative next-nearest-neighbor hopping $t'/t < 0$ (resembling hole-doped cuprates) and such with $t'/t > 0$ (electron doped): Whereas the hole-like Fermi surface curvature of the former is enhanced when approaching the insulating state for small dopings, the system is driven toward a nested Fermi surface in the latter.

5.2.2. Organizing principles: momentum-sector-selective metal-insulator transition, Widom line, and Fermi-surface topology.
Systematic DCA studies including variation of cluster sizes and doping (223) revealed a robust rationale for the perspective of the pseudogap regime in the $t - t'$ Hubbard model (where t' is introduced to distinguish electron from hole doping) as a doping-driven Mott transition (see **Figure 4a, ii**): in the heavily doped regime, nonlocal correlations are small, yielding a nearly isotropic Fermi liquid (in the sense that the quasiparticle lifetimes and weights at the Fermi surface are nearly constant). Reducing the doping toward half-filling introduces a substantial differentiation in momentum space between quasiparticles at the node and antinode, such that the shorter lifetimes occur near the antinodal point and the longest lifetimes occur at the nodal point. The system, however, remains consistent with Fermi liquid theory at any point on the Fermi surface. Reducing the doping further toward half-filling establishes a gap near the antinode while the node remains metallic. In cluster simulations, this is the momentum-dependent (sector-selective) transition that characterizes the pseudogap in the Hubbard model (224). Reducing doping to half-filling leads to a phase transition to a Mott insulator with a substantially larger and isotropic gap. On the electron-doped side, the sector-selective regime is smaller or, if t' is large enough, absent, and momentum differentiation is weaker. It has been argued (see, e.g., 218) that the key ingredient for the pseudogap is the proximity to the Mott transition rather than long-range AF fluctuations, which are believed to be the gapping mechanism on the electron-doped side. A two-site minimal model exhibiting a momentum-selective transition is presented in References 225 and 226.
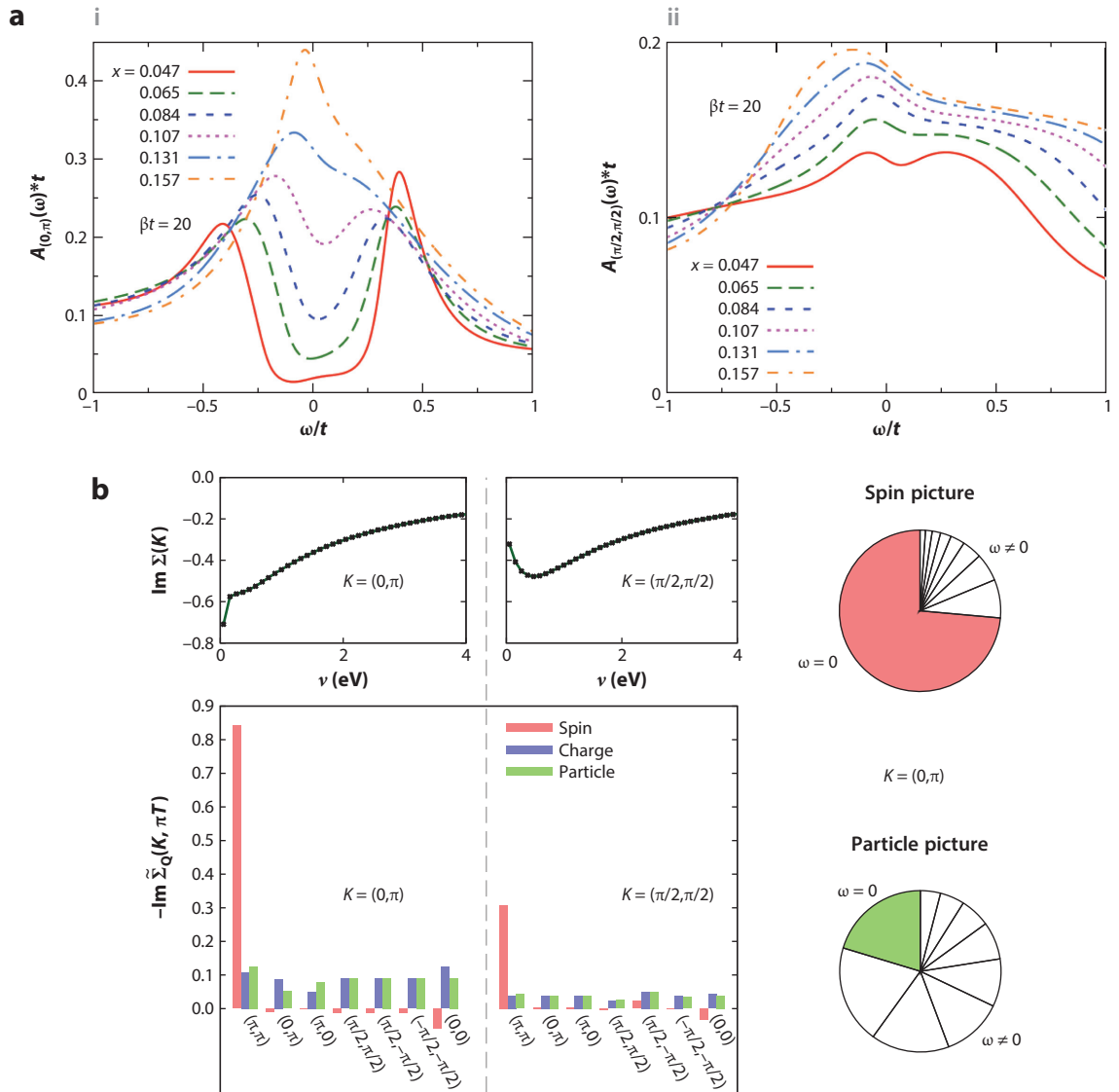
Figure 4

(*a*) Many-body density of states from an eight-site DCA calculation with $U/t = 7$, $t'/t = -0.15$, and $T/t = 0.05$ for various hole dopings x at the antinode and node, respectively. (*b*) Fluctuation diagnostics of a DCA self-energy in the pseudogap regime, showing that short-range spin fluctuations are the origin of the pseudogap in the 2D Hubbard model. Abbreviation: DCA, dynamical cluster approximation. Panel *a* adapted with permission from Reference 78; copyright 2010 American Physical Society. Panel *b* adapted with permission from Reference 217; copyright 2015 American Physical Society.

A different organizing principle has been suggested in 2×2 CDMFT clusters (227). There, several thermodynamic and dynamic determination criteria for T^* are found to collapse onto a line of thermodynamic anomalies that emanates from the critical endpoint of the Mott transition at finite doping. This is the so-called Widom line (228).

Conflicting interpretations exist on the influence of nesting and the van Hove singularity at strong coupling. Although eight-site DCA calculations find no substantial effect of the van Hove singularity on the pseudogap (224), DCA and determinantal quantum Monte Carlo (DQMC) simulations (137, 229) find substantial effects. The discrepancy remains unresolved.

5.2.3. Insights into the origin of the pseudogap via fluctuation diagnostic approaches.
Although observables such as the single-particle spectral function show signatures of the pseudogap, they do not easily reveal the underlying fluctuations that cause this feature. This analysis can be performed by examining the dominant fluctuations (charge, spin, or pairing) and their change upon entering the pseudogap regime. This technique is known as fluctuation diagnostics (217). The approach relies on the Dyson–Schwinger equation of motion, which relates the (one-particle) self-energy Σ to the (two-particle) scattering vertex F. Expressing this relation in different fluctuation channels, their (momentum- or frequency-resolved) contributions to the self-energy $\tilde{\Sigma}_{\mathbf{Q}/\Omega}$ can be determined. **Figure 4b** shows the self-energy and its fluctuation diagnostics calculated in DCA in a region of the 2D phase diagram where the Hubbard model exhibits a pseudogap. Although the momentum contributions $\tilde{\Sigma}_{\mathbf{Q}}$ in the charge and particle–particle channel are uniformly distributed over the momentum vectors considered, in the spin channel there is a clear peak visible at $\mathbf{Q} = (\pi, \pi)$. In frequency, only in the spin channel the zero-frequency contribution $\tilde{\Sigma}_{\Omega=0}$ dominates; i.e., only the spin fluctuations are long-lived. From these observations, one can conclude that well-defined short-ranged magnetic fluctuations lead to the opening of the pseudogap in the 2D Hubbard model. In Reference 141, a fully momentum-resolved fluctuation diagnostic has been performed with DiagMC data. The interplay of spin and charge fluctuations for wide parameter ranges has been computed in DCA in Reference 230. A systematic review of different types and applications of fluctuation diagnostic techniques can be found in Reference 91.

5.3. Superconductivity

The spontaneous emergence of superconducting pairing in a system with strong repulsive interactions has been one of the primary drivers for studying the model, and several earlier reviews (8–12) present the topic in detail. At weak coupling, a superconducting ground state (with several different superconducting symmetries) exists (45, 115, 121, 122; see Section 4.1). However, as mentioned in Section 5.1, in a substantial parameter regime around $U/t \sim 8$ and for moderate doping, the phase is preempted by various types of stripes. Nevertheless, superconductivity is very close in energy to those states, and minor changes in the model, such as additional nonlocal hoppings or interactions, may drive it to a superconducting state. The investigation of this superconducting state and its relationship to the pseudogap, charge-ordered, and metallic states remains an important topic of active research.

The superconducting phase boundary can be determined in two ways: upon cooling from the high-temperature disordered phase by tracking the divergence of the superconducting susceptibility or upon heating from the low-T phase by investigating the disappearance of the superconducting order parameter. With normal state calculations, early QMC results on finite-size clusters found $d_{x^2-y^2}$ as the most likely pairing symmetry in the Hubbard model for moderate doping (231). Large-cluster simulations with extrapolations could be performed in DCA (48) and the critical temperature determined, and Reference 232 explored the parameter regimes most conducive to superconductivity.

Cluster DMFT simulations directly in the ordered superconducting state have been performed by several groups on four-site (see, e.g., 171, 227, 233–235) and eight-site dynamical mean-field

clusters (236, 237). These simulations allow analysis of the nature and properties of the super-conducting state (including energetics, spectral functions, gap functions, and other response functions), in addition to determining the phase boundary. Although considerable finite-size effects remain, generic trends such as the energetics of the model or the evolution of response functions coincide with other methods and observations on cuprate materials.

Of considerable interest has been the pairing mechanism of the model. Several works (117, 238), including studies with DCA (239–243), found that AF fluctuations play the role of pairing glue in the model. In Reference 244, the influence of the dynamical vertex structure on the superconducting transition temperature has been analyzed within the DΓA, and particle–particle scattering processes have been identified as one of the main oppressors of T_c.

5.4. Bad Metal

The model at high temperature and intermediate doping is metallic, but transport properties are inconsistent with Fermi liquid behavior. The characterization of the temperature dependence of the resistivity, which is believed to be linear in temperature over a wide range of temperatures, and of other transport properties in this regime has been a matter of recent attention. Results are available from various methods, including linked cluster expansion (245), DMFT (245–248), and lattice MC (249).

Calculating the resistivity is technically difficult. The interpretation of finite-temperature results on the Matsubara axis, such as those obtained by continuous-time QMC dynamical mean field solvers or lattice MC methods, is complicated by the fact that analytical continuation is unreliable at high temperature, due to the distance of the Matsubara points from the real axis, and the fact that the spacing of Matsubara points changes linearly in T, thereby introducing a systematic uncertainty into any temperature dependence. Current real frequency formulations, such as those based on DMFT [using numerical renormalization group (NRG; 247, 250) or exact diagonalization (ED; 248) as impurity solver], neglect vertex corrections (251). Thus, though the regime at very high temperature is well understood, there is an intermediate temperature regime where currently no reliable calculations exist. Modern DiagMC methods formulated in real frequency (252) promise a resolution of this problem (see also 253).

6. TOWARD THE SIMULATION OF EXPERIMENTAL PROBES

6.1. Angle-Resolved Photoemission Spectroscopy

Much less is known about single- and two-particle excitations in the intermediate-to-strong coupling regime than about the energetics and the phase diagram of the model. The spectral function is directly observable in photoemission experiments. Up to matrix elements, it corresponds to the imaginary part of the retarded real frequency Green's function, which can be obtained from finite-temperature methods (working on the imaginary frequency or imaginary time axis) via analytic continuation (64, 254). However, the continuation kernel is ill conditioned, and uncertainties or stochastic noise on the imaginary axis are amplified exponentially, leading to unreliable spectral functions especially at high temperature, away from zero frequency, and for bosonic quantities. Thus, though features such as the existence of a gap or a quasiparticle peak are typically robust, there is considerable uncertainty in the numerical value of gap sizes or peak heights.

Cluster methods (10) have been used to obtain spectral functions at select points in k-space. Interpolation methods for the Green's function, self-energy, or cumulants (255) can then be employed to obtain continuous k-space Green's functions and extract quasiparticle weights or Fermi

surfaces. Special care must be taken to disentangle interpolation artifacts from data. In three dimensions, results from cluster DMFT (93) and lattice MC (256) are available.

Several aspects of the spectral function can be obtained without resorting to analytical continuation. For instance, the imaginary time quantity $\beta G(\beta/2)$ converges to the density of states at the Fermi energy for $T \to 0$ (257), and quasiparticle weights, gap sizes, or the location of metal-to-insulator transitions are accessible from fits of the Matsubara self-energy (77, 223).

6.2. Optical Conductivities

Within linear response theory, the response of a model to a weak external field is described by a two-particle correlation function consisting of a product of single-particle Green's functions and its vertex correction (258).

The response to an externally applied electric field corresponds to a current-current correlation function (259). In the simulation of a layered 2D system, the c-axis contribution is proportional to a product of two single-particle Green's functions and the interplane hopping, and no vertex corrections appear (78, 260). Interplane conductivities show a clear signature of the pseudogap opening with temperature and doping, consistent with experiments on the cuprates. In contrast, the evaluation of the in-plane conductivity requires vertex corrections (78, 261), which only disappear in single-site (262) and four-site CDMFT (263) due to symmetry. Results for conductivities are available from cluster DMFT at low T and single-site DMFT and high-temperature series expansion (245) as well as Lanczos (251) at high T. Cluster methods find a large insulating gap in the undoped system, a Drude peak with 'mid-IR' feature upon doping, and a clear Drude peak in the metallic regime (78).

6.3. Raman Spectroscopy

Electronic Raman spectroscopy (264, 265) is a versatile photon-in-photon-out technique used to probe correlations in correlated electron systems. Depending on the polarization of the incoming and outgoing light, different areas of the Brillouin zone are probed. On a square 2D lattice, two main light polarizations of interest are B_{1g} [sensitive to areas around (π, π)] and B_{2g} [highlighting $(\pi/2, \pi/2)$].

Simulated Raman results on the 2D model are available from cluster DMFT, with (266) and without (78, 267) vertex corrections, as well as in the superconducting state (268). They show a two-magnon Raman peak in the insulator, signatures of the pseudogap upon doping, and a temperature-and-doping evolution generally consistent with experiment.

6.4. Magnetic Response

Simulating the full momentum- and energy-dependent magnetic susceptibility or structure factor, such as it would be measured by neutron spectroscopy, is an important open problem. Lattice and quantum cluster methods do not have enough momentum resolution to capture the momentum resolution in an unbiased way, and results therefore come from approximate methods such as dual fermions (269, 270). These results can be directly compared with neutron spectroscopy on the cuprates (32).

Quantum cluster methods are better suited to simulating the local magnetic susceptibility, as it is measured, e.g., in NMR. Results for the Knight shift, spin–echo decay time, and relaxation rates are presented in (271) and show the characteristic suppression of the NMR Knight shift in the pseudogap regime, along with a differentiation between oxygen and copper relaxation rates.

7. GENERALIZATIONS AND EXTENSIONS

7.1. The Two-Dimensional Hubbard Model on Other Lattices

We so far have discussed the Hubbard model on the square and cubic lattices. The model displays additional interesting properties on lattices that are not square. In particular, the interplay between frustration and correlation may lead to exotic magnetism at half-filling, and doping holes may result in additional exotic electronic states.

7.1.1. Honeycomb lattice.

The model on the honeycomb lattice is studied mostly because of its connection to graphene. The lattice is bipartite but has a Fermi surface that is very different from that of the square lattice. At half-filling, the Fermi surface shrinks to two Dirac points, which causes AF order to appear only when U is larger than a critical value U_c (272). This makes the model an ideal playground to study the interaction-driven metal-insulator transition. At half-filling, due to the absence of the sign problem, the model can be efficiently studied with QMC. It is now well established that there is a direct phase transition from a Dirac semimetal to an AF Mott insulator at a critical $U_c/t \approx 3.8$ (273, 274; and no intermediate spin liquid phase). The phase transition is in the Gross–Neveu–Yukawa universality class (274–276). Away from half-filling, much attention was paid to one-quarter doping, where the Fermi surface has a nesting feature. Nesting in a Fermi surface usually triggers an instability toward an ordered state in the weak interaction region. Chiral $d + id$ superconducting order was found by several groups using a variety of methods (277–279).

7.1.2. Triangular lattice.

The triangular lattice is the simplest lattice with geometric frustration and may be relevant for certain organic materials (280). At half-filling, 120-deg magnetic order was confirmed by different methods (281, 282) in the Heisenberg model. The evolution of the phase diagram with U at half-filling is still under debate (see 270, 283, 284, and references therein). In the most recent DMRG study on an infinite cylinder (283), a chiral spin liquid phase was found between the metallic phase at weak interaction and the 120-deg magnetically ordered phase at strong interaction. However, the latest VMC study (284) did not find evidence of an intermediate spin liquid phase, except upon adding a sufficiently large t'. More studies of large systems with high accuracy are needed to resolve this controversy. At finite temperatures, a multimethod study of the metal-to-insulator crossover has been recently performed (285), where increased chiral correlations coexisting with stripy AF correlations at intermediate coupling strengths have also been found. Progress in computing frequency-dependent magnetic and charge susceptibilities has been achieved based on the ladder dual fermion approximation (270).

7.1.3. Kagome lattice.

The kagome lattice is another commonly studied lattice with geometrical frustration. Unlike other lattices discussed here, no magnetic order is found at half-filling in the strongly interacting limit, and there is a growing consensus that the ground state is a quantum spin liquid (see 286, and references therein). The Mott transition at half-filling was studied in Reference 287 with cluster DMFT, where a critical coupling $U_c/t \sim 8.22$ was found. In Reference 288, a Wigner crystal state was found in the lightly doped t-J model based on DMRG. The investigation of the physics at larger doping is still underway. In Reference 289, a multimethod study using DQMC, DMFT, and DΓA investigated the magnetic correlations across the Mott transition.

7.2. The Attractive Model

The attractive ($U < 0$) Hubbard model is often used as a model system for electronic superconductivity and superconducting phase transitions. On bipartite lattices, the attractive interaction

can be transformed to a repulsive one with a partial particle–hole transformation: $\hat{c}_{i\uparrow} \rightarrow \hat{d}_{i\uparrow}, \hat{c}_{i\downarrow} \rightarrow (-1)^i \hat{d}_{i\downarrow}^\dagger$. With this transformation, the spin-balanced attractive Hubbard model at arbitrary filling is mapped to a spin-imbalanced repulsive Hubbard model at half-filling.

QMC methods do not suffer from a sign problem here, and therefore accurate calculations of very large system sizes at low temperature are possible (290). At half-filling, onsite s-wave pairing and charge-density wave order at (π, π) coexist (50), which corresponds to the AF Néel order in the spin-balanced repulsive Hubbard model at half-filling. Away from half-filling, only the on-site pairing survives, and the model displays a KT phase transition at finite temperature. The KT transition temperature goes to zero as the system approaches half-filling (61, 290; see 291 for its accurate determination). Furthermore, superconductivity can be significantly enhanced if the Fermi energy is close to a logarithmic van Hove singularity in the density of states (292). The attractive Hubbard model remains sign-problem free even with a Rashba spin–orbit coupling (293).

7.3. Multiorbital Models

One may envisage an approach that gradually, in a bottom-up manner, adds more and more orbitals and interactions to the model until the full electronic structure Hamiltonian is recovered. A first step along this route leads to multiorbital models with local Hubbard interactions. The number of possible models quickly grows, and parameter choices become material specific. Cuprate physics has inspired the three-orbital Emery (203, 294) or p-d model, motivated by a downfolding of electronic structure to three, instead of one, orbitals, and the bilayer Hubbard model (295). For a discussion of competing ground states in the three-orbital model, see Section 5.1.3. Oxide perovskites have been studied in three-orbital generalizations of the Hubbard model. Typically, interorbital Slater–Kanamori terms that are not of the density–density type are also included (296). These interactions are characterized by three parameters: U, U', and J. The model, most often studied with single-site multiorbital DMFT, has given rise to the so-called Hund's metals (297). The joint application of band downfolding techniques and treatment of the resulting low-energy multiorbital model with DMFT [DFT (density functional theory)+DMFT] is a frequently used strategy for the description of realistic materials (298).

7.4. Models with Nonlocal Interactions

Instead of adding additional orbitals with local interactions, one may consider adding additional nonlocal interactions to the single-orbital Hubbard model. The simplest step along this route leads to the extended Hubbard model, where a repulsive nearest-neighbor density–density term V is added to the local U. The extended Hubbard model is a paradigmatic model for charge order, as the system is driven to a charge-ordered state as V is increased and the temperature is lowered, leading to an interplay of charge order, correlation, antiferromagnetism, metallic behavior, and Mott insulating behavior. For this reason, the system has been studied within DCA (299–302), where these interactions are treated explicitly, as well as within the so-called dual boson approach (21, 303), where they are treated in a diagrammatic expansion around DMFT.

7.5. Nonequilibrium and Driven System

Real-time dependence of Hubbard models outside of linear response is a topic that has recently found much interest. Nonequilibrium can occur in many varieties, including quantum quenches (where parameters of the model are suddenly changed), the coupling to an external driving field (such as an electromagnetic field in a pump–probe setup), or the application of a voltage and the evaluation of currents in the short-time transient or long-time steady-state limit. In the long-time

limit, there is a question of thermalization to a steady state or to equilibrium, and there are interesting questions on the destruction and reestablishment of ordered phases and of nonequilibrium phases (304).

Reliable and generic numerical tools for these setups are mostly absent, and developing them is a field with great promise. Single-site and small-cluster dynamical mean-field calculations have been performed for most of these setups (305). Floquet systems (i.e., systems exposed to a periodic drive) have also been studied in cold atomic gas setups (306, 307).

8. CONCLUSIONS AND PERSPECTIVES

In summary, thanks to substantial advances with different computational methods in recent years, controlled numerical solutions of the Hubbard model in various regions of the phase diagram have become available. This has led to a consensus on several aspects of the model. For example, the long-standing controversy over stripe states has been resolved, and it is now widely accepted that they are the ground state over an extended doping, interaction, and t' range. Similarly, there is a consensus that the pseudogap at strong coupling is caused by strong short-range AF fluctuations.

Despite all of this progress, there remain many open challenges, such as determining the precise locations of phase boundaries (in particular, the parameter region with d-wave superconductivity), investigating the role of phase separation at low doping with more methods, and understanding the interplay of superconductivity and stripe order in partially filled stripes. Another open problem is the accurate study of the competition between stripe and uniform phases at finite temperature, which will be important to connect the current ground state results (mostly from wave-function-based methods) with the finite-temperature results (predominantly from Green's function–based approaches). More accurate techniques beyond single-site DMFT for transport calculations (e.g., fully vertex-corrected resistivities) are needed to fully reveal the physics of the high-temperature metallic regime, which so far has remained largely unexplored by numerical approaches. Similarly, more direct and controlled access to real-time evolution and real frequency observables is an essential future direction. The physics of models with more orbitals and/or longer-ranged interactions remains largely unexplored with accurate methods, and reliable algorithms have yet to be developed. Such methods will be essential to connect calculations on the single-band model to multiband Hubbard models and electronic structure Hamiltonians without resorting to crude downfolding techniques.

In view of these rapid advances, the prospects of addressing some of these issues in the near future seem promising. For example, tensor network simulations in two dimensions have recently been extended to finite temperature (see, e.g., 308–310) and have already been used to study the onset of stripe correlations at $\delta = 1/16$ doping (308). More finite-temperature results in other parameter regimes as well as excitation spectra (65, 76, 311, 312) from tensor network approaches can be expected in the future. Progress in computing dynamical quantities has also recently been achieved by dynamical VMC approaches (313, 314), with a first application to the 2D Hubbard model in Reference 314. Furthermore, diagrammatic approaches based on the two-particle vertex are being extended to real frequencies (315).

Finite-temperature methods have similarly made rapid progress. Recent years have seen the advent of large-cluster dynamical mean-field studies that could be extrapolated to the thermodynamic limit in practice, extensions of the DMFT that became more and more accurate, and the emergence of continuous-time and DiagMC methods that are orders of magnitude more powerful than previous techniques.

The development of new, generally applicable numerical techniques that overcome the shortcomings of existing methods therefore remains the most urgent need for addressing the

open issues. Although this article did not focus on technical aspects of these calculations, most of the advances achieved over the past 15 years can be traced directly back to algorithmic and numerical progress.

DISCLOSURE STATEMENT

The authors are not aware of any affiliations, memberships, funding, or financial holdings that might be perceived as affecting the objectivity of this review.

ACKNOWLEDGMENTS

LITERATURE CITED

1. Hubbard J. 1963. *Proc. R. Soc. Lond. Ser. A* 276(1365):238–57
2. Kanamori J. 1963. *Prog. Theor. Phys.* 30(3):275–89
3. Gutzwiller MC. 1963. *Phys. Rev. Lett.* 10(5):159–62
4. Gull E, Millis AJ. 2015. *Nat. Phys.* 11(10):808–10
5. LeBlanc JPF, Antipov AE, Becca F, Bulik IW, Chan GKL, et al. 2015. *Phys. Rev. X* 5(4):041041
6. Schäfer T, Wentzell N, Šimkovic F, He YY, Hille C, et al. 2021. *Phys. Rev. X* 11(1):011058
7. Chubukov AV. 1993. *Phys. Rev. B* 48(2):1097–104
8. Dagotto E. 1994. *Rev. Mod. Phys.* 66(3):763–840
9. Bulut N. 2002. *Adv. Phys.* 51(7):1587–667
10. Maier T, Jarrell M, Pruschke T, Hettler MH. 2005. *Rev. Mod. Phys.* 77(3):1027–80
11. Tremblay AMS, Kyung B, Sénéchal D. 2006. *Low Temp. Phys.* 32(4):424–51
12. Scalapino DJ. 2007. In *Handbook of High-Temperature Superconductivity*, ed. JR Schrieffer, pp. 495–526. New York: Springer
13. Scalapino DJ. 2012. *Rev. Mod. Phys.* 84(4):1383–417
14. Arovas DP, Berg E, Kivelson SA, Raghu S. 2022. *Annu. Rev. Condens. Matter Phys.* 13:239–74
15. Daré AM, Albinet G. 2000. *Phys. Rev. B* 61(7):4567–75
16. Staudt R, Dzierzawa M, Muramatsu A. 2000. *Eur. Phys. J. B* 17(3):411–15
17. Rohringer G, Toschi A, Katanin A, Held K. 2011. *Phys. Rev. Lett.* 107(25):256402
18. Kent PRC, Jarrell M, Maier TA, Pruschke T. 2005. *Phys. Rev. B* 72(6):060411
19. Hirschmeier D, Hafermann H, Gull E, Lichtenstein AI, Antipov AE. 2015. *Phys. Rev. B* 92(14):144409
20. Kozik E, Burovski E, Scarola VW, Troyer M. 2013. *Phys. Rev. B* 87(20):205102
21. Rohringer G, Hafermann H, Toschi A, Katanin AA, Antipov AE, et al. 2018. *Rev. Mod. Phys.* 90(2):025003. **https://doi.org/10.1103/RevModPhys.90.025003**
22. Andersen O, Liechtenstein A, Jepsen O, Paulsen F. 1995. *J. Phys. Chem. Solids* 56(12):1573–91
23. Pavarini E, Dasgupta I, Saha-Dasgupta T, Jepsen O, Andersen OK. 2001. *Phys. Rev. Lett.* 87(4):047003
24. Zheng H, Changlani HJ, Williams KT, Busemeyer B, Wagner LK. 2018. *Front. Phys.* 6:43
25. Hirayama M, Yamaji Y, Misawa T, Imada M. 2018. *Phys. Rev. B* 98(13):134501
26. Hirayama M, Misawa T, Ohgoe T, Yamaji Y, Imada M. 2019. *Phys. Rev. B* 99(24):245155
27. Damascelli A, Hussain Z, Shen ZX. 2003. *Rev. Mod. Phys.* 75(2):473–541
28. Hybertsen MS, Schlüter M, Christensen NE. 1989. *Phys. Rev. B* 39(13):9028–41

29. Zhang FC, Rice TM. 1988. *Phys. Rev. B* 37(7):3759–61
30. Markiewicz RS, Sahrakorpi S, Lindroos M, Lin H, Bansil A. 2005. *Phys. Rev. B* 72(5):054519
31. Kim C, White PJ, Shen ZX, Tohyama T, Shibata Y, et al. 1998. *Phys. Rev. Lett.* 80(19):4245–48
32. Coldea R, Hayden SM, Aeppli G, Perring TG, Frost CD, et al. 2001. *Phys. Rev. Lett.* 86(23):5377–80
33. Kitatani M, Si L, Janson O, Arita R, Zhong Z, Held K. 2020. *npj Quantum Mater.* 5(1):59
34. Powell BJ, McKenzie RH. 2006. *J. Phys. Condens. Matter* 18(45):R827–66
35. Georgescu IM, Ashhab S, Nori F. 2014. *Rev. Mod. Phys.* 86(1):153–85
36. Mazurenko A, Chiu CS, Ji G, Parsons MF, Kanász-Nagy M, et al. 2017. *Nature* 545(7655):462–66
37. Byrnes T, Kim NY, Kusudo K, Yamamoto Y. 2008. *Phys. Rev. B* 78(7):075320
38. Singha A, Gibertini M, Karmakar B, Yuan S, Polini M, et al. 2011. *Science* 332(6034):1176–79
39. Hensgens T, Fujita T, Janssen L, Li X, Van Diepen CJ, et al. 2017. *Nature* 548(7665):70–73
40. Schneider U, Hackermüller L, Ronzheimer JP, Will S, Braun S, et al. 2012. *Nat. Phys.* 8(3):213–18
41. White IG, Hulet RG, Hazzard KRA. 2019. *Phys. Rev. A* 100(3):033612
42. Somma R, Ortiz G, Gubernatis JE, Knill E, Laflamme R. 2002. *Phys. Rev. A* 65(4):042323
43. Arute F, Arya K, Babbush R, Bacon D, Bardin JC, et al. 2020. arXiv:2010.07965
44. Wecker D, Hastings MB, Wiebe N, Clark BK, Nayak C, Troyer M. 2015. *Phys. Rev. A* 92(6):062318
45. Deng Y, Kozik E, Prokof'ev NV, Svistunov BV. 2015. *Europhys. Lett.* 110(5):57001
46. Šimkovic F, Liu XW, Deng Y, Kozik E. 2016. *Phys. Rev. B* 94(8):085106
47. Mermin ND, Wagner H. 1966. *Phys. Rev. Lett.* 17(22):1133–36. Erratum. 1966. *Phys. Rev. Lett.* 17:1307–8
48. Maier TA, Jarrell M, Schulthess TC, Kent PRC, White JB. 2005. *Phys. Rev. Lett.* 95(23):237001
49. Fradkin E, Kivelson SA, Tranquada JM. 2015. *Rev. Mod. Phys.* 87(2):457–82
50. Hirsch JE. 1985. *Phys. Rev. B* 31(7):4403–19
51. Hirsch JE, Tang S. 1989. *Phys. Rev. Lett.* 62(5):591–94
52. White SR, Scalapino DJ, Sugar RL, Loh EY, Gubernatis JE, Scalettar RT. 1989. *Phys. Rev. B* 40(1):506–16
53. Varney CN, Lee CR, Bai ZJ, Chiesa S, Jarrell M, Scalettar RT. 2009. *Phys. Rev. B* 80(7):075116
54. Dagotto E, Moreo A, Ortolani F, Poilblanc D, Riera J. 1992. *Phys. Rev. B* 45(18):10741–60
55. Qin M, Shi H, Zhang S. 2016. *Phys. Rev. B* 94(8):085103
56. Qin M, Shi H, Zhang S. 2017. *Phys. Rev. B* 96(7):075156
57. Kim AJ, Simkovic F, Kozik E. 2020. *Phys. Rev. Lett.* 124(11):117602
58. Prokof'ev NV, Svistunov BV. 1998. *Phys. Rev. Lett.* 81(12):2514–17
59. Lenihan C, Kim AJ, Šimkovic F IV, Kozik E. 2021. *Phys. Rev. Lett.* 126(10):105701
60. Chakravarty S, Halperin BI, Nelson DR. 1988. *Phys. Rev. Lett.* 60(11):1057–60
61. Moreo A, Scalapino DJ. 1991. *Phys. Rev. Lett.* 66(7):946–48
62. Schäfer T, Geles F, Rost D, Rohringer G, Arrigoni E, et al. 2015. *Phys. Rev. B* 91(12):125109
63. Rohringer G, Toschi A. 2016. *Phys. Rev. B* 94(12):125144
64. Jarrell M, Gubernatis J. 1996. *Phys. Rep.* 269(3):133–95
65. Van Damme M, Vanhove R, Haegeman J, Verstraete F, Vanderstraeten L. 2021. *Phys. Rev. B* 104:115142
66. Furukawa N, Imada M. 1992. *J. Phys. Soc. Jpn.* 61(9):3331–54
67. Assaad FF, Imada M. 1996. *Phys. Rev. Lett.* 76(17):3176–79
68. Vitali E, Shi H, Qin M, Zhang S. 2016. *Phys. Rev. B* 94(8):085140
69. Yang C, Feiguin AE. 2016. *Phys. Rev. B* 93(8):081107
70. White SR. 1992. *Phys. Rev. Lett.* 69:2863
71. Bulut N, Scalapino DJ, White SR. 1994. *Phys. Rev. Lett.* 72(5):705–8
72. Preuss R, Hanke W, von der Linden W. 1995. *Phys. Rev. Lett.* 75(7):1344–47
73. Preuss R, Hanke W, Gröber C, Evertz HG. 1997. *Phys. Rev. Lett.* 79(6):1122–25
74. Gröber C, Eder R, Hanke W. 2000. *Phys. Rev. B* 62(7):4336–52
75. Schollwöck U. 2011. *Ann. Phys.* 326:96–192
76. Bohrdt A, Demler E, Pollmann F, Knap M, Grusdt F. 2020. *Phys. Rev. B* 102(3):035139
77. Georges A, Kotliar G, Krauth W, Rozenberg MJ. 1996. *Rev. Mod. Phys.* 68(1):13–125
78. Lin N, Gull E, Millis AJ. 2010. *Phys. Rev. B* 82(4):045104. **https://doi.org/10.1103/PhysRevB.82.045104**

79. Klett M, Wentzell N, Schäfer T, Simkovic F, Parcollet O, et al. 2020. *Phys. Rev. Res.* 2(3):033476
80. Šimkovic F, LeBlanc JPF, Kim AJ, Deng Y, Prokof'ev NV, et al. 2020. *Phys. Rev. Lett.* 124(1):017003
81. Mott NF. 1949. *Proc. Phys. Soc. Sect. A* 62(7):416–22
82. Anderson PW. 1959. *Phys. Rev.* 115(1):2–13
83. Anderson P. 1997. *Adv. Phys.* 46(1):3–11
84. Slater JC. 1951. *Phys. Rev.* 82(4):538–41
85. Gull E, Werner P, Wang X, Troyer M, Millis AJ. 2008. *Europhys. Lett.* 84(3):37009
86. Moukouri S, Jarrell M. 2001. *Phys. Rev. Lett.* 87(16):167010
87. Manousakis E. 1991. *Rev. Mod. Phys.* 63(1):1–62
88. Sandvik AW, Evertz HG. 2010. *Phys. Rev. B* 82(2):024407
89. Borejsza K, Dupuis N. 2004. *Phys. Rev. B* 69(8):085119
90. Fradkin E. 2013. *Field Theories of Condensed Matter Physics*. Cambridge, UK: Cambridge Univ. Press, 2nd ed.
91. Schäfer T, Toschi A. 2021. *J. Phys. Condens. Matter* 33(21):214001
92. Scalettar RT, Scalapino DJ, Sugar RL, Toussaint D. 1989. *Phys. Rev. B* 39(7):4711–14
93. Fuchs S, Gull E, Troyer M, Jarrell M, Pruschke T. 2011. *Phys. Rev. B* 83(23):235113
94. Blankenbecler R, Scalapino DJ, Sugar RL. 1981. *Phys. Rev. D* 24(8):2278–86
95. Gull E, Millis AJ, Lichtenstein AI, Rubtsov AN, Troyer M, Werner P. 2011. *Rev. Mod. Phys.* 83(2):349–404
96. Paiva T, Loh YL, Randeria M, Scalettar RT, Trivedi N. 2011. *Phys. Rev. Lett.* 107(8):086401
97. Fuchs S, Gull E, Pollet L, Burovski E, Kozik E, et al. 2011. *Phys. Rev. Lett.* 106(3):030401
98. Schäfer T, Katanin AA, Held K, Toschi A. 2017. *Phys. Rev. Lett.* 119(4):046402
99. Jaksch D, Zoller P. 2005. *Ann. Phys.* 315(1):52–79
100. Esslinger T. 2010. *Annu. Rev. Condens. Matter Phys.* 1:129–52
101. Jördens R, Tarruell L, Greif D, Uehlinger T, Strohmaier N, et al. 2010. *Phys. Rev. Lett.* 104(18):180401
102. Greif D, Uehlinger T, Jotzu G, Tarruell L, Esslinger T. 2013. *Science* 340(6138):1307–10
103. Hart RA, Duarte PM, Yang TL, Liu X, Paiva T, et al. 2015. *Nature* 519(7542):211–14
104. Ibarra-García-Padilla E, Mukherjee R, Hulet RG, Hazzard KRA, Paiva T, Scalettar RT. 2020. *Phys. Rev. A* 102(3):033340
105. Schulz HJ. 1990. *Phys. Rev. Lett.* 64(12):1445–48
106. Dombre T. 1990. *J. Phys. France* 51(9):847–56
107. Frésard R, Dzierzawa M, Wölfle P. 1991. *Europhys. Lett.* 15(3):325–30
108. Igoshev PA, Timirgazin MA, Katanin AA, Arzhnikov AK, Irkhin VY. 2010. *Phys. Rev. B* 81(9):094407
109. Shraiman BI, Siggia ED. 1989. *Phys. Rev. Lett.* 62(13):1564–67
110. Chubukov AV, Frenkel DM. 1992. *Phys. Rev. B* 46(18):11884–901
111. Chubukov AV, Musaelian KA. 1995. *Phys. Rev. B* 51(18):12605–17
112. Kotov VN, Sushkov OP. 2004. *Phys. Rev. B* 70(19):195105
113. Halboth CJ, Metzner W. 2000. *Phys. Rev. Lett.* 85(24):5162–65
114. Husemann C, Salmhofer M. 2009. *Phys. Rev. B* 79(19):195125
115. Metzner W, Salmhofer M, Honerkamp C, Meden V, Schönhammer K. 2012. *Rev. Mod. Phys.* 84(1):299–352
116. Yamase H, Eberlein A, Metzner W. 2016. *Phys. Rev. Lett.* 116(9):096402
117. Scalapino D. 1995. *Phys. Rep.* 250(6):329–65
118. Bickers NE, Scalapino DJ, White SR. 1989. *Phys. Rev. Lett.* 62(8):961–64
119. Neumayr A, Metzner W. 2003. *Phys. Rev. B* 67(3):035112
120. Kyung B, Landry JS, Tremblay AMS. 2003. *Phys. Rev. B* 68(17):174502
121. Raghu S, Kivelson SA, Scalapino DJ. 2010. *Phys. Rev. B* 81(22):224505
122. Šimkovic F IV, Deng Y, Kozik E. 2021. *Phys. Rev. B* 104:L020507
123. Zanchi D, Schulz HJ. 2000. *Phys. Rev. B* 61(20):13609–32
124. Honerkamp C, Salmhofer M, Furukawa N, Rice TM. 2001. *Phys. Rev. B* 63(3):035109
125. Honerkamp C, Salmhofer M. 2001. *Phys. Rev. Lett.* 87(18):187004
126. Eberlein A, Metzner W. 2014. *Phys. Rev. B* 89(3):035126

127. Reiss J, Rohe D, Metzner W. 2007. *Phys. Rev. B* 75(7):075110
128. Wang J, Eberlein A, Metzner W. 2014. *Phys. Rev. B* 89(12):121116
129. Irkhin VY, Katanin AA, Katsnelson MI. 2001. *Phys. Rev. B* 64(16):165107
130. Hlubina R, Sorella S, Guinea F. 1997. *Phys. Rev. Lett.* 78(7):1343–46
131. Katanin AA, Kampf AP. 2003. *Phys. Rev. B* 68(19):195101
132. Vilardi D, Bonetti PM, Metzner W. 2020. *Phys. Rev. B* 102(24):245128
133. Taranto C, Andergassen S, Bauer J, Held K, Katanin A, et al. 2014. *Phys. Rev. Lett.* 112(19):196402
134. Vilardi D, Taranto C, Metzner W. 2019. *Phys. Rev. B* 99(10):104501
135. Vilk YM, Tremblay AMS. 1997. *J. Phys. I France* 7(11):1309–68
136. Kyung B, Hankevych V, Daré AM, Tremblay AMS. 2004. *Phys. Rev. Lett.* 93(14):147004
137. Wu W, Scheurer MS, Chatterjee S, Sachdev S, Georges A, Ferrero M. 2018. *Phys. Rev. X* 8(2):021048
138. van Loon EGCP, Hafermann H, Katsnelson MI. 2018. *Phys. Rev. B* 97(8):085125
139. Eckhardt CJ, Honerkamp C, Held K, Kauch A. 2020. *Phys. Rev. B* 101(15):155104
140. Hille C, Rohe D, Honerkamp C, Andergassen S. 2020. *Phys. Rev. Res.* 2(3):033068
141. Wu W, Ferrero M, Georges A, Kozik E. 2017. *Phys. Rev. B* 96(4):041105
142. Sénéchal D, Tremblay AMS. 2004. *Phys. Rev. Lett.* 92(12):126401
143. Vojta M. 2009. *Adv. Phys.* 58(6):699–820
144. Kloss T, Montiel X, Carvalho VS, Freire H, Pépin C. 2016. *Rep. Prog. Phys.* 79(8):084507
145. Agterberg DF, Davis JS, Edkins SD, Fradkin E, Van Harlingen DJ, et al. 2020. *Annu. Rev. Condens. Matter Phys.* 11:231–70
146. Tranquada JM, Sternlieb BJ, Axe JD, Nakamura Y, Uchida S. 1995. *Nature* 375(6532):561–63
147. Zaanen J, Gunnarsson O. 1989. *Phys. Rev. B* 40(10):7391–94
148. Poilblanc D, Rice TM. 1989. *Phys. Rev. B* 39(13):9749–52
149. Machida K. 1989. *Phys. C: Superconduct.* 158(1–2):192–96
150. Schulz H. 1989. *J. Phys.* 50(18):2833–49
151. Kato M, Machida K, Nakanishi H, Fujita M. 1990. *J. Phys. Soc. Jpn.* 59:1047–58
152. White SR, Scalapino DJ. 1998. *Phys. Rev. Lett.* 80(6):1272–75
153. White SR, Scalapino DJ. 1998. *Phys. Rev. Lett.* 81(15):3227–30
154. White SR, Scalapino DJ. 2003. *Phys. Rev. Lett.* 91(13):136403
155. White SR, Scalapino DJ. 1999. *Phys. Rev. B* 60(2):R753–56
156. Himeda A, Kato T, Ogata M. 2002. *Phys. Rev. Lett.* 88(11):117001
157. White SR, Scalapino DJ. 2009. *Phys. Rev. B* 79(22):220504
158. Corboz P, White SR, Vidal G, Troyer M. 2011. *Phys. Rev. B* 84(4):041108
159. Corboz P, Rice TM, Troyer M. 2014. *Phys. Rev. Lett.* 113(4):046402
160. Zheng BX, Chan GKL. 2016. *Phys. Rev. B* 93(3):035126
161. Berg E, Fradkin E, Kim EA, Kivelson SA, Oganesyan V, et al. 2007. *Phys. Rev. Lett.* 99(12):127003
162. Li Q, Hücker M, Gu GD, Tsvelik AM, Tranquada JM. 2007. *Phys. Rev. Lett.* 99(6):067001
163. Raczkowski M, Capello M, Poilblanc D, Frésard R, Oles AM. 2007. *Phys. Rev. B* 76(14):140505
164. Yokoyama H, Shiba H. 1988. *J. Phys. Soc. Jpn.* 57(7):2482–93
165. Gros C. 1988. *Phys. Rev. B* 38(1):931–34
166. Giamarchi T, Lhuillier C. 1991. *Phys. Rev. B* 43(16):12943–51
167. Sorella S, Martins GB, Becca F, Gazza C, Capriotti L, et al. 2002. *Phys. Rev. Lett.* 88(11):117002
168. Eichenberger D, Baeriswyl D. 2007. *Phys. Rev. B* 76(18):180504
169. Misawa T, Imada M. 2014. *Phys. Rev. B* 90(11):115137
170. Tocchio LF, Becca F, Sorella S. 2016. *Phys. Rev. B* 94(19):195126
171. Lichtenstein AI, Katsnelson MI. 2000. *Phys. Rev. B* 62(14):R9283–86
172. Capone M, Kotliar G. 2006. *Phys. Rev. B* 74(5):054513
173. Becca F, Capriotti L, Sorella S. 2001. *Phys. Rev. Lett.* 87(16):167005
174. Hu WJ, Becca F, Sorella S. 2012. *Phys. Rev. B* 85(8):081110
175. Jordan J, Orús R, Vidal G, Verstraete F, Cirac JI. 2008. *Phys. Rev. Lett.* 101(25):250602
176. Zhang S, Carlson J, Gubernatis JE. 1997. *Phys. Rev. B* 55(12):7464–77
177. Chang CC, Zhang S. 2010. *Phys. Rev. Lett.* 104(11):116402

178. Peters R, Kawakami N. 2014. *Phys. Rev. B* 89(15):155134
179. Knizia G, Chan GKL. 2012. *Phys. Rev. Lett.* 109(18):186404
180. Zheng BX, Chung CM, Corboz P, Ehlers G, Qin MP, et al. 2017. *Science* 358(6367):1155–60
181. Ido K, Ohgoe T, Imada M. 2018. *Phys. Rev. B* 97(4):045138
182. Tocchio LF, Montorsi A, Becca F. 2019. *SciPost Phys.* 7(2):021
183. Huang EW, Mendl CB, Jiang HC, Moritz B, Devereaux TP. 2018. *npj Quantum Mater.* 3(1):22
184. Ehlers G, White SR, Noack RM. 2017. *Phys. Rev. B* 95:125125
185. Jiang HC, Devereaux TP. 2019. *Science* 365(6460):1424–28
186. Jiang YF, Zaanen J, Devereaux TP, Jiang HC. 2020. *Phys. Rev. Res.* 2(3):033073
187. Sorella S. 2021. arXiv:2101.07045 [cond-mat]
188. Darmawan AS, Nomura Y, Yamaji Y, Imada M. 2018. *Phys. Rev. B* 98(20):205132
189. Simons Collab. on the Many-Electron Problem, Qin M, Chung CM, Shi H, Vitali E, et al. 2020. *Phys. Rev. X* 10(3):031016
190. Emery VJ, Kivelson SA, Lin HQ. 1990. *Phys. Rev. Lett.* 64(4):475–78
191. White SR, Scalapino DJ. 2000. *Phys. Rev. B* 61(9):6320–26
192. Ohgoe T, Hirayama M, Misawa T, Ido K, Yamaji Y, Imada M. 2020. *Phys. Rev. B* 101(4):045124
193. Ponsioen B, Chung SS, Corboz P. 2019. *Phys. Rev. B* 100(19):195141
194. Simons Collab. on the Many-Electron Problem, Chung CM, Qin M, Zhang S, Schollwöck U, White SR. 2020. *Phys. Rev. B* 102(4):041106
195. Dodaro JF, Jiang HC, Kivelson SA. 2017. *Phys. Rev. B* 95(15):155116
196. Jiang HC, Weng ZY, Kivelson SA. 2018. *Phys. Rev. B* 98(14):140505
197. Yanagisawa T, Koike S, Yamaji K. 2001. *Phys. Rev. B* 64(18):184509
198. Yanagisawa T, Miyazaki M, Yamaji K. 2009. *J. Phys. Soc. Jpn.* 78(1):013706
199. Weber C, Giamarchi T, Varma CM. 2014. *Phys. Rev. Lett.* 112(11):117001
200. Zegrodnik M, Biborski A, Fidrysiak M, Spałek J. 2019. *Phys. Rev. B* 99(10):104511
201. Biborski A, Zegrodnik M, Spałek J. 2020. *Phys. Rev. B* 101(21):214504
202. Zegrodnik M, Biborski A, Fidrysiak M, Spałek J. 2021. *J. Phys. Condens. Matter* 33:415601
203. Cui ZH, Sun C, Ray U, Zheng BX, Sun Q, Chan GKL. 2020. *Phys. Rev. Res.* 2(4):043259
204. Weber C, Yee C, Haule K, Kotliar G. 2012. *Europhys. Lett.* 100(3):37001
205. Mai P, Balduzzi G, Johnston S, Maier TA. 2021. *Phys. Rev. B* 103(14):144514
206. White SR, Scalapino DJ. 2015. *Phys. Rev. B* 92(20):205112
207. Huang EW, Mendl CB, Liu S, Johnston S, Jiang HC, et al. 2017. *Science* 358(6367):1161–64
208. Chiciak A, Vitali E, Zhang S. 2020. *Phys. Rev. B* 102(21):214512
209. Alloul H, Ohno T, Mendels P. 1989. *Phys. Rev. Lett.* 63(16):1700–3
210. Hüfner S, Hossain MA, Damascelli A, Sawatzky GA. 2008. *Rep. Prog. Phys.* 71(6):062501
211. Kanigel A, Norman MR, Randeria M, Chatterjee U, Souma S, et al. 2006. *Nat. Phys.* 2(7):447–51
212. Shen KM, Ronning F, Lu DH, Baumberger F, Ingle NJC, et al. 2005. *Science* 307(5711):901–4
213. Kastner MA, Birgeneau RJ, Shirane G, Endoh Y. 1998. *Rev. Mod. Phys.* 70(3):897–928
214. Maier T, Jarrell M, Pruschke T, Keller J. 2000. *Eur. Phys. J. B Condens. Matter Complex Syst.* 13(4):613–24
215. Huscroft C, Jarrell M, Maier T, Moukouri S, Tahvildarzadeh AN. 2001. *Phys. Rev. Lett.* 86(1):139–42
216. Macridin A, Jarrell M, Maier T, Kent PRC, D'Azevedo E. 2006. *Phys. Rev. Lett.* 97(3):036401
217. Gunnarsson O, Schäfer T, LeBlanc JPF, Gull E, Merino J, et al. 2015. *Phys. Rev. Lett.* 114(23):236402. **https://doi.org/10.1103/PhysRevLett.114.236402**
218. Parcollet O, Biroli G, Kotliar G. 2004. *Phys. Rev. Lett.* 92(22):226402
219. Civelli M, Capone M, Kancharla SS, Parcollet O, Kotliar G. 2005. *Phys. Rev. Lett.* 95(10):106402
220. Kyung B, Kancharla SS, Sénéchal D, Tremblay AMS, Civelli M, Kotliar G. 2006. *Phys. Rev. B* 73(16):165114
221. Zhang YZ, Imada M. 2007. *Phys. Rev. B* 76(4):045108
222. Liebsch A, Tong NH. 2009. *Phys. Rev. B* 80(16):165126
223. Gull E, Ferrero M, Parcollet O, Georges A, Millis AJ. 2010. *Phys. Rev. B* 82(15):155101
224. Gull E, Parcollet O, Werner P, Millis AJ. 2009. *Phys. Rev. B* 80(24):245102
225. Ferrero M, Cornaglia PS, De Leo L, Parcollet O, Kotliar G, Georges A. 2009. *Phys. Rev. B* 80(6):064501

226. Ferrero M, Cornaglia PS, De Leo L, Parcollet O, Kotliar G, Georges A. 2009. *Europhys. Lett.* 85(5):57009
227. Sordi G, Sémon P, Haule K, Tremblay AMS. 2012. *Phys. Rev. Lett.* 108(21):216401
228. Terletska H, Vuččević J, Tanasković D, Dobrosavljević V. 2011. *Phys. Rev. Lett.* 107(2):026401
229. Wu W, Scheurer MS, Ferrero M, Georges A. 2020. *Phys. Rev. Res.* 2(3):033067
230. Dong X, Gull E. 2020. *Phys. Rev. B* 101(19):195115
231. White SR, Scalapino DJ, Sugar RL, Bickers NE, Scalettar RT. 1989. *Phys. Rev. B* 39(1):839–42
232. Chen X, LeBlanc JPF, Gull E. 2015. *Phys. Rev. Lett.* 115(11):116402
233. Maier TA, Jarrell M, Macridin A, Slezak C. 2004. *Phys. Rev. Lett.* 92(2):027005
234. Haule K, Kotliar G. 2007. *Phys. Rev. B* 76(10):104509
235. Civelli M. 2009. *Phys. Rev. B* 79(19):195113
236. Gull E, Parcollet O, Millis AJ. 2013. *Phys. Rev. Lett.* 110(21):216405
237. Gull E, Millis AJ. 2012. *Phys. Rev. B* 86(24):241106
238. Monthoux P, Balatsky AV, Pines D. 1991. *Phys. Rev. Lett.* 67(24):3448–51
239. Maier TA, Jarrell MS, Scalapino DJ. 2006. *Phys. Rev. Lett.* 96(4):047005
240. Maier TA, Jarrell M, Scalapino DJ. 2006. *Phys. Rev. B* 74(9):094513
241. Maier TA, Jarrell M, Scalapino DJ. 2007. *Phys. Rev. B* 75(13):134519
242. Maier TA, Macridin A, Jarrell M, Scalapino DJ. 2007. *Phys. Rev. B* 76(14):144516
243. Gull E, Millis AJ. 2014. *Phys. Rev. B* 90(4):041110
244. Kitatani M, Schäfer T, Aoki H, Held K. 2019. *Phys. Rev. B* 99(4):041115
245. Perepelitsky E, Galatas A, Mravlje J, Žitko R, Khatami E, et al. 2016. *Phys. Rev. B* 94(23):235115
246. Pruschke T, Jarrell M, Freericks J. 1995. *Adv. Phys.* 44(2):187–210
247. Deng X, Mravlje J, Žitko R, Ferrero M, Kotliar G, Georges A. 2013. *Phys. Rev. Lett.* 110(8):086401
248. Cha P, Patel AA, Gull E, Kim EA. 2020. *Phys. Rev. Res.* 2(3):033434
249. Huang EW, Sheppard R, Moritz B, Devereaux TP. 2019. *Science* 366(6468):987–90
250. Bulla R, Costi TA, Pruschke T. 2008. *Rev. Mod. Phys.* 80(2):395–450
251. Vučičević J, Kokalj J, Žitko R, Wentzell N, Tanasković D, Mravlje J. 2019. *Phys. Rev. Lett.* 123(3):036601
252. Taheridehkordi A, Curnoe SH, LeBlanc JPF. 2020. *Phys. Rev. B* 102(4):045115
253. Vučičević J, Ferrero M. 2020. *Phys. Rev. B* 101(7):075113
254. Fei J, Yeh CN, Gull E. 2021. *Phys. Rev. Lett.* 126(5):056402
255. Stanescu TD, Kotliar G. 2006. *Phys. Rev. B* 74(12):125110
256. Ulmke M, Scalettar RT, Nazarenko A, Dagotto E. 1996. *Phys. Rev. B* 54(23):16523–32
257. Trivedi N, Randeria M. 1995. *Phys. Rev. Lett.* 75(2):312–15
258. Rohringer G, Valli A, Toschi A. 2012. *Phys. Rev. B* 86(12):125114
259. Basov DN, Timusk T. 2005. *Rev. Mod. Phys.* 77(2):721–79
260. Ferrero M, Parcollet O, Georges A, Kotliar G, Basov DN. 2010. *Phys. Rev. B* 82(5):054502
261. Lin N, Gull E, Millis AJ. 2009. *Phys. Rev. B* 80(16):161105
262. Jarrell M, Freericks JK, Pruschke T. 1995. *Phys. Rev. B* 51(17):11704–11
263. Haule K, Kotliar G. 2007. *Europhys. Lett.* 77(2):27007
264. Le Tacon M, Sacuto A, Georges A, Kotliar G, Gallais Y, et al. 2006. *Nat. Phys.* 2(8):537–43
265. Devereaux TP, Hackl R. 2007. *Rev. Mod. Phys.* 79(1):175–233
266. Lin N, Gull E, Millis AJ. 2012. *Phys. Rev. Lett.* 109(10):106401
267. Sakai S, Blanc S, Civelli M, Gallais Y, Cazayous M, et al. 2013. *Phys. Rev. Lett.* 111(10):107001
268. Gull E, Millis AJ. 2013. *Phys. Rev. B* 88(7):075127
269. LeBlanc JPF, Li S, Chen X, Levy R, Antipov AE, et al. 2019. *Phys. Rev. B* 100(7):075123
270. Li S, Gull E. 2020. *Phys. Rev. Res.* 2(1):013295
271. Chen X, Leblanc JPF, Gull E. 2017. *Nat. Commun.* 8:14986
272. Sorella S, Tosatti E. 1992. *Europhys. Lett.* 19(8):699–704
273. Sorella S, Otsuka Y, Yunoki S. 2012. *Sci. Rep.* 2(1):992
274. Assaad FF, Herbut IF. 2013. *Phys. Rev. X* 3(3):031010
275. Herbut IF. 2006. *Phys. Rev. Lett.* 97(14):146401
276. Otsuka Y, Yunoki S, Sorella S. 2016. *Phys. Rev. X* 6(1):011029
277. Nandkishore R, Levitov LS, Chubukov AV. 2012. *Nat. Phys.* 8(2):158–63

278. Wang WS, Xiang YY, Wang QH, Wang F, Yang F, Lee DH. 2012. *Phys. Rev. B* 85(3):035414
279. Gu ZC, Jiang HC, Sheng DN, Yao H, Balents L, Wen XG. 2013. *Phys. Rev. B* 88(15):155112
280. Kanoda K, Kato R. 2011. *Annu. Rev. Condens. Matter Phys.* 2:167–88
281. Capriotti L, Trumper AE, Sorella S. 1999. *Phys. Rev. Lett.* 82(19):3899–902
282. White SR, Chernyshev AL. 2007. *Phys. Rev. Lett.* 99(12):127004
283. Szasz A, Motruk J, Zaletel MP, Moore JE. 2020. *Phys. Rev. X* 10(2):021042
284. Tocchio LF, Montorsi A, Becca F. 2020. *Phys. Rev. B* 102(11):115150
285. Wietek A, Rossi R, Šimkovic F IV, Klett M, Hansmann P, et al. 2021. *Phys. Rev. X* 11:041013
286. Liao HJ, Xie ZY, Chen J, Liu ZY, Xie HD, et al. 2017. *Phys. Rev. Lett.* 118(13):137202
287. Ohashi T, Kawakami N, Tsunetsugu H. 2006. *Phys. Rev. Lett.* 97(6):066401
288. Jiang HC, Devereaux T, Kivelson SA. 2017. *Phys. Rev. Lett.* 119(6):067002
289. Kaufmann J, Steiner K, Scalettar RT, Held K, Janson O. 2021. *Phys. Rev. B* 104:165127
290. Scalettar RT, Loh EY, Gubernatis JE, Moreo A, White SR, et al. 1989. *Phys. Rev. Lett.* 62(12):1407–10
291. Paiva T, dos Santos RR, Scalettar RT, Denteneer PJH. 2004. *Phys. Rev. B* 69(18):184501
292. Hirsch JE, Scalapino DJ. 1986. *Phys. Rev. Lett.* 56(25):2732–35
293. Shi H, Rosenberg P, Chiesa S, Zhang S. 2016. *Phys. Rev. Lett.* 117(4):040401
294. Emery VJ. 1987. *Phys. Rev. Lett.* 58(26):2794–97
295. Maier TA, Scalapino DJ. 2011. *Phys. Rev. B* 84(18):180513
296. Imada M, Fujimori A, Tokura Y. 1998. *Rev. Mod. Phys.* 70(4):1039–263
297. Georges A, de' Medici L, Mravlje J. 2013. *Annu. Rev. Condens. Matter Phys.* 4:137–78
298. Kotliar G, Savrasov SY, Haule K, Oudovenko VS, Parcollet O, Marianetti CA. 2006. *Rev. Mod. Phys.* 78(3):865–951
299. Terletska H, Chen T, Gull E. 2017. *Phys. Rev. B* 95(11):115149
300. Terletska H, Chen T, Paki J, Gull E. 2018. *Phys. Rev. B* 97(11):115117
301. Jiang M, Hähner UR, Schulthess TC, Maier TA. 2018. *Phys. Rev. B* 97(18):184507
302. Paki J, Terletska H, Iskakov S, Gull E. 2019. *Phys. Rev. B* 99(24):245146
303. Stepanov EA, Peters L, Krivenko IS, Lichtenstein AI, Katsnelson MI, Rubtsov AN. 2018. *npj Quantum Mater.* 3:54
304. Oka T, Kitamura S. 2019. *Annu. Rev. Condens. Matter Phys.* 10:387–408
305. Aoki H, Tsuji N, Eckstein M, Kollar M, Oka T, Werner P. 2014. *Rev. Mod. Phys.* 86(2):779–837
306. Messer M, Sandholzer K, Görg F, Minguzzi J, Desbuquois R, Esslinger T. 2018. *Phys. Rev. Lett.* 121(23):233603
307. Sandholzer K, Murakami Y, Görg F, Minguzzi J, Messer M, et al. 2019. *Phys. Rev. Lett.* 123(19):193602
308. Wietek A, He YY, White SR, Georges A, Stoudenmire EM. 2021. *Phys. Rev. X* 11:031007
309. Czarnik P, Dziarmaga J, Corboz P. 2019. *Phys. Rev. B* 99(3):035115
310. Chen B-B, Chen C, Chen Z, Cui J, Zhai Y, et al. 2021. *Phys. Rev. B* 103(4):L041107
311. Vanderstraeten L, Haegeman J, Verstraete F. 2019. *Phys. Rev. B* 99(16):165121
312. Ponsioen B, Corboz P. 2020. *Phys. Rev. B* 101(19):195109
313. Ferrari F, Becca F. 2019. *Phys. Rev. X* 9(3):031026
314. Charlebois M, Imada M. 2020. *Phys. Rev. X* 10(4):041023
315. Kugler FB, Lee SSB, von Delft J. 2021. *Phys. Rev. X* 11:041006